

GenAI-Powered Inference*

Kosuke Imai[†]

Kentaro Nakamura[‡]

July 8, 2025

Abstract

We introduce GenAI-Powered Inference (GPI), a statistical framework for both causal and predictive inference using unstructured data, including text and images. GPI leverages open-source Generative Artificial Intelligence (GenAI) models—such as large language models and diffusion models—not only to generate unstructured data at scale but also to extract low-dimensional representations that capture their underlying structure. Applying machine learning to these representations, GPI enables estimation of causal and predictive effects while quantifying associated estimation uncertainty. Unlike existing approaches to representation learning, GPI does not require fine-tuning of generative models, making it computationally efficient and broadly accessible. We illustrate the versatility of the GPI framework through three applications: (1) analyzing Chinese social media censorship, (2) estimating predictive effects of candidates’ facial appearance on electoral outcomes, and (3) assessing the persuasiveness of political rhetoric. An open-source software package is available for implementing GPI.

Key Words: deep generative models, double machine learning, generative artificial intelligence, large language models, representation learning, unstructured data

*An open-source Python package, GPI: **GenAI-Powered Inference**, that implements the proposed methodology is available at <https://gpi-pack.github.io/>.

[†]Professor, Department of Government and Department of Statistics, Harvard University, Cambridge, MA 02138. Phone: 617-384-6778, Email: Imai@Harvard.Edu, URL: <https://imai.fas.harvard.edu>

[‡]Ph.D. student, John F. Kennedy School of Government, Harvard University. Email: knakamura@g.harvard.edu

1 Introduction

The emergence of Generative Artificial Intelligence (GenAI), including large language models and diffusion models, has transformed many aspects of society. In this paper, we show that GenAI can also serve as a powerful tool for causal and predictive inference. We introduce a new statistical framework, *GenAI-Powered Inference* (GPI), which leverages open-source GenAI models to enhance statistical analysis with high-dimensional unstructured data such as text and images.

This paper illustrates the power of GPI through the following three applications:

1. **Text as confounder:** Estimating causal effects of a treatment by adjusting for latent confounders embedded in textual data
2. **Predictive effects of image features:** Assessing the predictive impact of specific image features while adjusting for other relevant characteristics in the same image.
3. **Structural model of texts:** Estimating structural models that incorporate both observed and latent textual features as covariates.

A common challenge in these settings is that while high-dimensional unstructured data are observed, we do not know, *a priori*, which features serve as relevant confounders.

GPI addresses this challenge by leveraging the ability of GenAI to generate or replicate unstructured data and to extract low-dimensional vector representations. Machine learning is then applied to these representations to identify a *deconfounder*, which is a summary of confounding information. Because these representations were used in the actual generative process, GPI eliminates the need to explicitly model the data-generating process or fine-tune the underlying GenAI models. This makes GPI a broadly accessible framework. Our open-source Python package GPI, which is available at <https://gpi-pack.github.io/>, implements the proposed methodology, further enhancing its applicability.

1.1 The Proposed Methodological Framework

Before moving on to each application, we provide a brief overview of the proposed methodology. Figure 1 considers two illustrative settings, in which the goal is to estimate the causal effect of treatment T on an outcome Y . The treatment may represent some features of unstructured data \mathbf{X} as in the “text / image as treatment” case (bottom right) or other variables as in the “text / image as confounder” case (top right). In both settings, the treatment-outcome relationship is confounded by the latent features \mathbf{U} of the unstructured data \mathbf{X} as well as other observed confounders \mathbf{Z} . A key challenge is to identify these latent confounding features \mathbf{U} and adjust for them to estimate causal effects.

To achieve its goal, GPI leverages GenAI models to produce unstructured data \mathbf{X} and extract corresponding internal representations \mathbf{R} . For existing texts or images, the GenAI model is prompted to regenerate the same content, enabling the derivation of consistent internal representations. Using \mathbf{R} rather than directly modeling the raw data \mathbf{X} offers three key advantages. First, \mathbf{R} is a significantly lower-dimensional embedding of the original high-dimensional input. Second, it encodes rich, relevant information distilled from the extensive data used during the GenAI model’s training. Third, by ensuring that the GenAI model is open-source and operates deterministically, GPI facilitates scientific replicability.

We then apply machine learning to the internal representation \mathbf{R} to estimate a deconfounder $f(\mathbf{R})$, which is a low-dimensional function that approximates the latent confounding structure \mathbf{U} and is sufficient for causal effect estimation. This step is critical because directly controlling for high-dimensional unstructured data \mathbf{X} can violate the positivity assumption and lead to biased

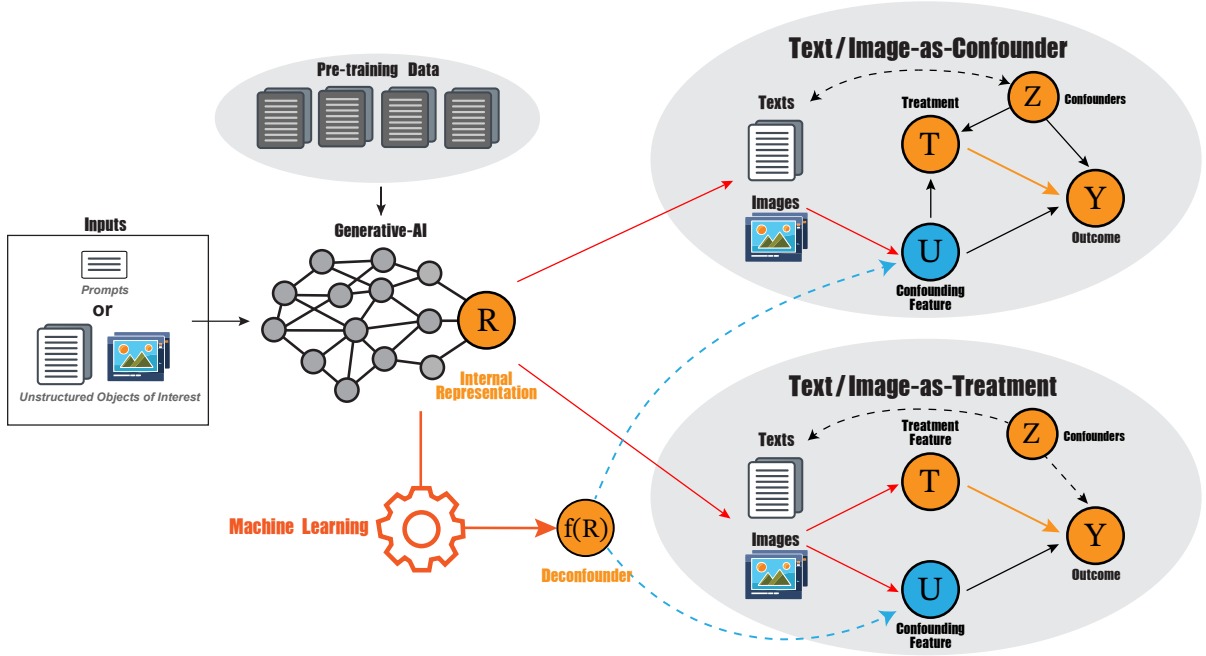


Figure 1: Illustration of GenAI-Powered Inference. Inputs to generative AI are either prompts or unstructured data (e.g., text or images). Pre-trained models produce internal representations \mathbf{R} , which we use to improve inference in two settings: (1) when text/images act as confounders, and (2) when they act as treatments. In the first setting (top right), the treatment-outcome relation is confounded by latent features of unstructured data \mathbf{U} and observed covariates \mathbf{Z} . In the second setting (bottom right), T depends on unstructured data and is similarly confounded. Since \mathbf{U} is unobserved, we apply machine learning to internal representation \mathbf{R} to learn a deconfounder $\mathbf{f}(\mathbf{R})$, a low-dimensional summary that enables unbiased causal inference without modeling the generative process or fine-tuning the GenAI model.

inference (D’Amour et al., 2021). While the deconfounder is not necessarily unique, we formally show that any valid $\mathbf{f}(\mathbf{R})$ enables nonparametric identification of causal effects when adjusted for alongside observed confounders \mathbf{Z} . We propose estimating the deconfounder using a deep neural network architecture designed to encode these necessary properties. The appendix provides theoretical justifications tailored to each application setting.

1.2 Related Work

A growing body of work addresses causal inference with unstructured high-dimensional data, often by either estimating low-dimensional embeddings (e.g., Veitch et al., 2020; Pryzant et al., 2021; Gui and Veitch, 2023; Klaassen et al., 2024) or modeling the data-generating process using parametric methods such as topic models (e.g., Fong and Grimmer 2016; Mozer et al. 2020; Roberts et al. 2020; Ahrens et al. 2021; Egami et al. 2022). These approaches typically rely on strong assumptions, such as the bag-of-words model and fixed embedding schemes, and face substantial challenges due to the statistical and computational complexity of high-dimensional unstructured data. This often leads to biased estimates and unreliable inference.

GPI departs from this paradigm by leveraging the internal representations of GenAI models, which inherently encode rich semantic information about the generated data and eliminate the

need to explicitly model or estimate representations. Further, GPI adopts a fully nonparametric approach by using neural networks to estimate the deconfounder, outcome model, and propensity score model, thereby avoiding restrictive functional form assumptions. This combination of principled representation learning and model flexibility enables more robust causal inference in complex, high-dimensional settings.

2 Applications

We demonstrate the wide applicability of GPI by reanalyzing three studies under the proposed framework: (1) estimating the causal effect of government censorship experience on the subsequent censorship or self-censorship (Roberts et al., 2020), (2) estimating the predictive effects of candidates’ facial appearance on electoral outcomes (Lindholm et al., 2024), and (3) estimating the persuasiveness of the political rhetoric (Blumenau and Lauderdale, 2022).

2.1 Text as Confounder

Social scientists have documented that the Chinese government selectively censors its citizens’ social media posts (e.g., Bamman et al., 2012; King et al., 2013). Building on this literature, Roberts et al. (2020) investigated whether users whose posts are censored are more likely to face future censorship and whether they respond by engaging in self-censorship.

The authors analyzed data from 75,324 Weibo posts collected by the Weiboscope project (Fu et al., 2013), which captures posts in real time and later checks whether they have been removed. Each post serves as a focal post, and they constructed three outcome variables: (1) the number of posts made by the same user in the four weeks following the focal post, (2) the proportion of those posts that were censored during the same time period; and (3) the proportion of posts that went missing during the same four-week window. See Appendix S1 for the full details of the data preprocessing.

Because censored and uncensored posts differ systematically, a naive regression of these outcomes on the treatment variable (prior censorship) would yield biased causal estimates. To address this confounding bias, the original analysis adjusts for the content of the focal post, the post date, and each user’s prior censorship history. We adopt the same covariate adjustment strategy within the GPI framework.

We use two open-source large language models, LLaMA 3 with 8 billion parameters (Grattafiori et al., 2024) and Gemma 3 with 1 billion parameters (Mesnard et al., 2024), to regenerate each focal post and extract its internal representation. These representations are then used to jointly estimate the deconfounder and outcome model within a single neural network architecture. A separate neural network is used to estimate the propensity score, conditional on the estimated deconfounder and other observed confounders. Both architectures are fine-tuned using Optuna, an automated hyperparameter optimization framework (Akiba et al., 2019).

To estimate the average treatment effect on the treated (ATT), we apply double machine learning with two-fold cross-fitting (Chernozhukov et al., 2018). Standard errors are clustered at the user level, and extreme propensity scores are truncated following the method proposed by Dorn (2025). Theoretical justifications and further implementation details are provided in Appendix S1.

Figure 2 compares the results from GPI with those from the text matching approach used in the original analysis, which employed coarsened exact matching (Iacus et al., 2012) on estimates from the structural topic model (Roberts et al., 2016). For comparison, we apply GPI to both the matched sample (628 users, 879 posts) and the full sample (4,155 users; 75,324 posts). In contrast to the original analysis, GPI finds that prior censorship significantly reduces users’ subsequent posting activity, providing evidence of self-censorship. Moreover, GPI reveals a much stronger effect of prior censorship on the likelihood of future censorship. Lastly, GPI’s full-sample estimates

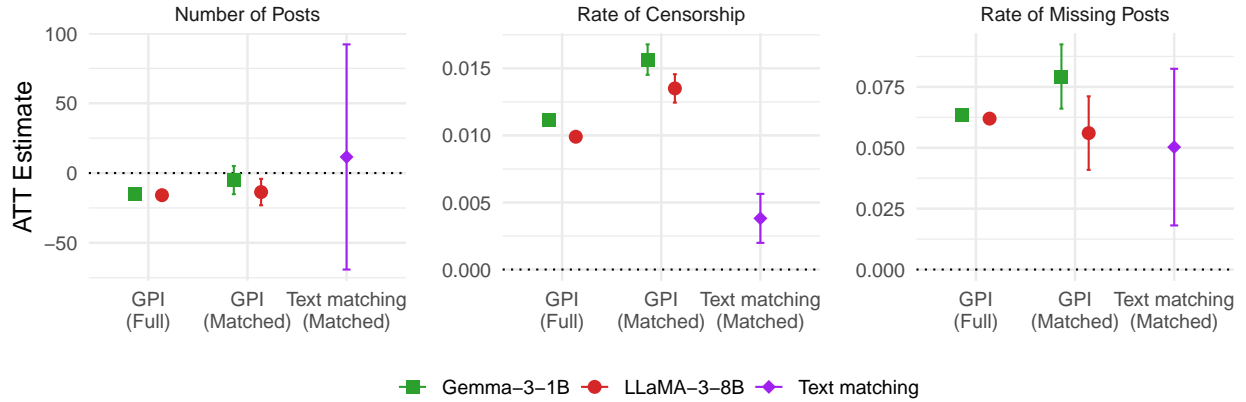


Figure 2: Estimated effects of prior censorship experience. For each outcome, we estimate the GPI results from LLaMA3 with 8 billion parameters (green) and Gemma3 with 1 billion parameters (red) using the full sample (Full) and the matched sample (Matched). We compare GPI estimates with those of the text matching approach used in the original analysis (purple). The interval bars represent 95% confidence intervals and the standard errors are clustered at the user level.

Outcome	GPI (LLaMA3-8B)		GPI (Gemma3-1B)		Text matching
	Full	Matched	Full	Matched	Matched
Number of posts	0.004 (0.273)	0.073 (0.094)	0.002 (0.532)	0.081 (0.061)	0.032 (0.398)
Rate of censorship	-0.001 (0.783)	-0.016 (0.587)	0.000 (0.925)	-0.024 (0.489)	0.089 (0.001)
Rate of missing posts	0.001 (0.735)	0.007 (0.826)	-0.000 (0.977)	0.042 (0.218)	0.062 (0.063)

Table 1: Pearson’s correlation (and associated p -value in parentheses) between the estimated efficient score of GPI and a candidate confounder (proportion of 60 censorship or self-censorship-related keywords). For text matching, the correlation between the candidate confounder and the residual from the implied weighted OLS is computed. If a method appropriately adjusts for the text features, then the correlation should be small and its p -value should be large. “Full” refers to the estimates using the entire sample while “Matched” refers to those based on the matched sample.

closely align with those from the matched sample, but are substantially more efficient, highlighting GPI’s advantages in both robustness and precision. These findings are consistent across both LLaMA 3 and Gemma 3 models.

To further illustrate GPI’s advantage, we assess covariate balance by computing the Pearson’s correlation between the estimated efficient score of GPI and a candidate confounder: the proportion of 60 censorship or self-censorship-related keywords identified by Fu et al. (2013). For text matching, we compute the Pearson’s correlation between this candidate confounder and the residuals from weighted OLS (with weights from coarsened exact matching). If a given method effectively adjusts for the confounding features in focal posts, it should yield a small correlation close to zero with a large p -value.

As shown in Table 1, GPI yields the correlations that are small in magnitude and have large p -values. In particular, the full sample analysis shows that the correlations are precisely estimated to be close to zero with large p -values. In contrast, the text matching approach produces a small p -value for the rate of censorship variable, despite its lower statistical power due to the limited size of matched sample, suggesting that residual confounding may still remain.

2.2 Predictive Effects of Image Features

Psychological research has long shown that people infer social attributes — such as trustworthiness or competence — from facial appearance (see e.g., Todorov et al., 2015). Building on this literature, Lindholm et al. (2024) examined whether facial appearance predicts electoral outcomes in Danish local and national elections. The authors compiled facial photographs of over 7,000 political candidates who ran for office in the 2021 local and 2022 general elections.

The primary predictors of interest are three facial traits previously identified as socially significant: attractiveness, trustworthiness, and competence (Sutherland et al., 2013). To quantify these traits, the authors fine-tuned a pre-trained convolutional neural network using the “One Million Impressions” dataset (Peterson et al., 2022). The outcome variable is the standardized number of votes (using z -scores) received by each candidate. The original analysis employed an ordinary least squares (OLS) regression of standardized vote counts on the three facial features, along with controls for age, gender, and education.

We apply GPI to this dataset and estimate the predictive effects of facial features, adjusting for both observed covariates and latent features embedded in facial appearance. While the original analysis did not account for such latent characteristics, candidate photos may contain additional visual cues that are predictive of electoral outcomes.

Each candidate photo is processed using two different versions of Stable Diffusion model (version 1.5 and 2.1) (Rombach et al., 2022) to extract its internal representation. We then estimate the deconfounder and outcome model using the same neural network architecture and fine-tuning procedure as in the previous application. Because the original predictors of interest — facial features — are continuous scores, we first discretize them based on 10 bins based on the sample quantiles and estimate the average predict effect at each bin. Theoretical justifications and implementation details are provided in Appendix S2.

Figure 3 compares the GPI estimates to the original OLS results, focusing on the sensitivity of predictive effects to covariate adjustment. Solid and dotted lines represent estimates with and without covariate adjustment, respectively, with blue and red shaded bands indicating the corresponding point-wise 95% confidence intervals. The GPI estimates exhibit greater robustness to the inclusion of covariates. Furthermore, GPI consistently finds that facial dominance is not statistically significantly associated with electoral outcomes, whereas the OLS results vary depending on whether covariates are included. This robustness likely reflects GPI’s ability to account for additional latent features present in candidates’ facial appearance. As before, these findings are consistent across GenAI models.

2.3 Structural Model of Texts

Political scientists and communication scholars have extensively studied the effectiveness of different rhetorical strategies (e.g., Jerit, 2009; Bos et al., 2013). Contributing this literature, Blumenau and Lauderdale (2022) conducted a forced-choice conjoint experiment to evaluate the persuasiveness of different types of political rhetoric. The authors constructed 336 political arguments by systematically varying 12 policy issues, 14 rhetorical elements, and position (support or opposition). Appendix S3 provides the full list of policy issues and rhetorical features.

A total of 3,317 participants were each shown four randomly assigned pairs of arguments.

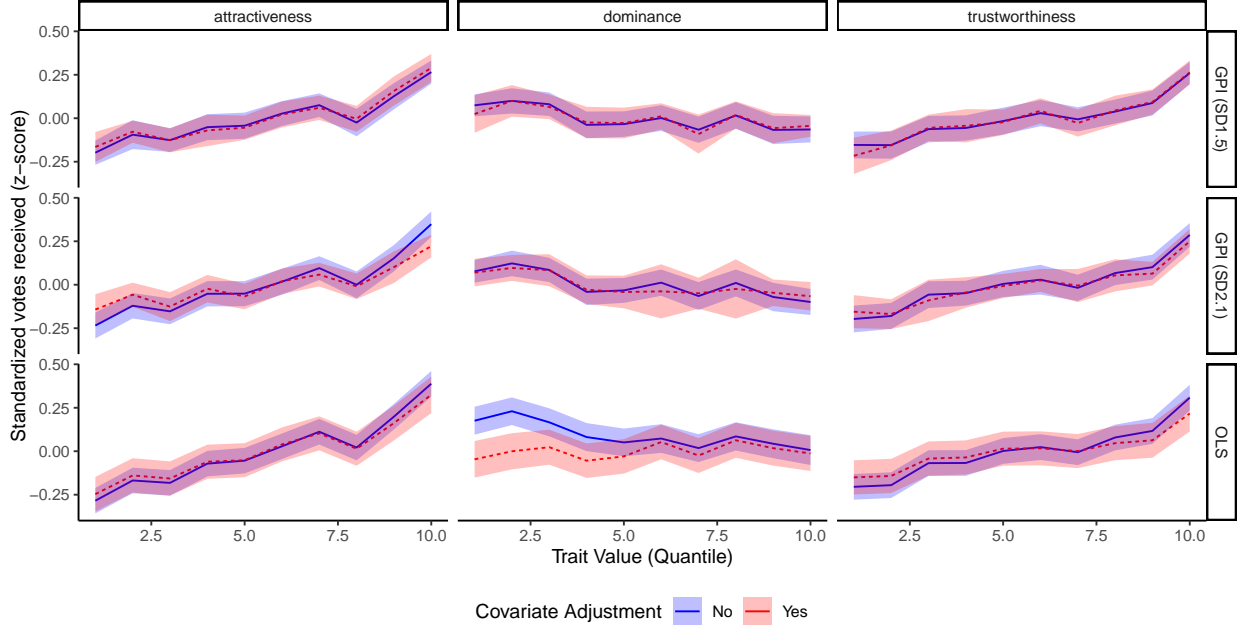


Figure 3: Estimated predictive effects of three facial traits (Attractiveness, Dominance, and Trustworthiness) using GPI with Stable Diffusion (SD) version 1.5 (top) and version 2.1 (middle) and OLS (bottom). In each panel, solid and dash lines represent estimates with and without covariate adjustment, respectively. Blue and red shaded areas indicate the corresponding 95% confidence intervals.

Within each pair, the arguments addressed the same policy issue but took opposite sides and featured different, randomly selected rhetorical elements. Participants were asked to indicate which argument they found more persuasive or whether both were equally persuasive, yielding a total of 13,268 pairwise comparisons. Appendix Table S3 provides one example pair of arguments.

The authors estimated the latent persuasiveness of rhetorical elements using a parametric structural model similar to the Bradley-Terry model (Bradley and Terry 1952; see Appendix Equation (S6)). This model assumes that the probability of one argument being judged more persuasive than another is determined by an additive combination of three effects: an interaction effect between policy area and position, the effect of the rhetorical element, and a random effect for each individual argument. The random effect accounts for unobserved features of the arguments that may influence persuasiveness but are not explicitly measured. In addition, the original analysis manually identified several potential confounders—such as argument length—and included them as covariates.

We use GPI to enhance the original analysis by relaxing its strong functional form assumptions. We compare the results based on three different LLMs: LLaMA3 with 8 billion parameters, along with two more recently released models — LLaMA3.3 with 70 billion parameters, and Gemma 3 with 1 billion parameters. While all these models are instruction-tuned and thus can be used to regenerate each argument and extract the internal representation, the internal representations are in different dimensions and contain different information. Our theoretical results imply that the results based on these models should be similar.

Once we extract internal representations, we then estimate a *semiparametric* version of the

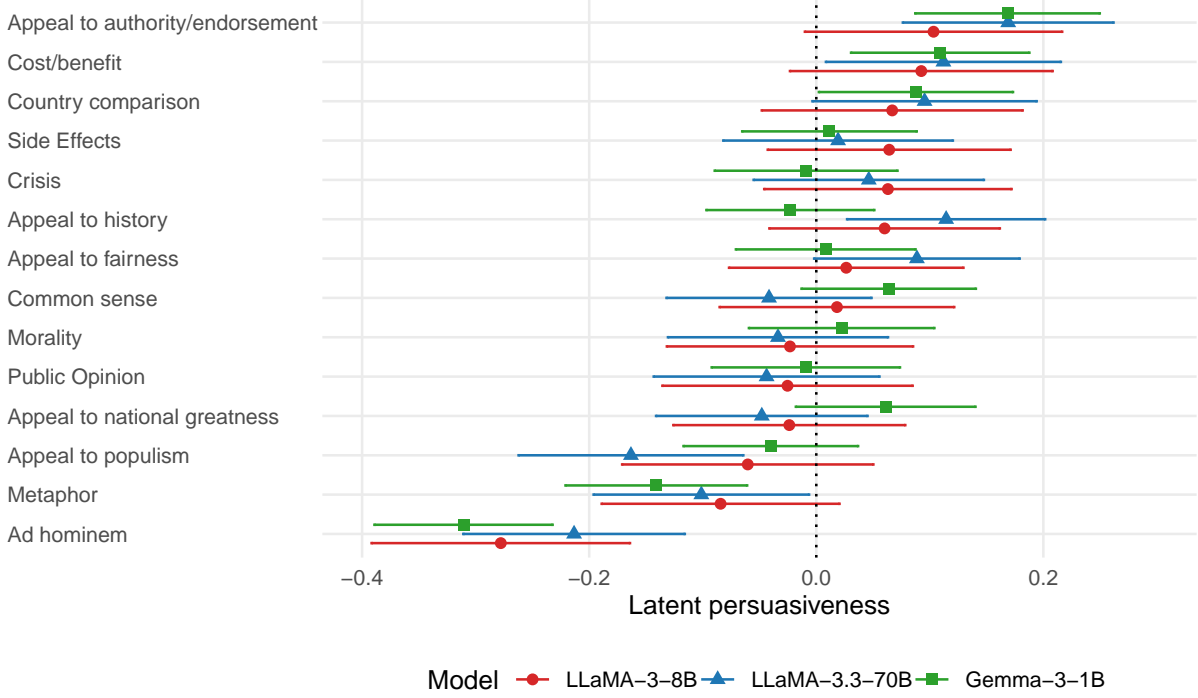


Figure 4: Estimated persuasiveness of 14 rhetorical elements in political arguments. We present the estimated latent persuasiveness based on LLaMA3 with 8 billion parameters (red circle), LLaMA3.3 with 70 billion parameters (blue triangle), and Gemma3 with 1 billion parameters (green rectangle). Each error bar represents the 95% confidence intervals obtained by Monte Carlo dropout.

original structural model, which allows for greater flexibility in capturing complex relationships,

$$\log \left[\frac{\mathbb{P}(Y_{jj'(i)} \leq k)}{\mathbb{P}(Y_{jj'(i)} > k)} \right] = \delta_k + \mu(T_j, \mathbf{U}_j) - \mu(T_{j'}, \mathbf{U}_{j'}) \quad (1)$$

where $Y_{jj'(i)} \in \{0, 1, 2\}$ denotes the relative persuasiveness of arguments j and j' shown to respondent i with 0 indicating that argument j is less persuasive than j' , 1 indicating equal persuasiveness, and 2 indicating argument j is more persuasive. The variable $T_j \in \{0, 1, \dots, 13\}$ denotes a rhetorical element used in argument j , and \mathbf{U}_j represents latent confounding features of that argument. Lastly, $\mu(T_j, \mathbf{U}_j)$ is a strength of the argument j , which is a nonparametric function of rhetorical element T_j and other confounding features \mathbf{U}_j . The original paper uses a special case of this semiparametric formulation, where $\mu(T_j, \mathbf{U}_j)$ is constrained to a linear-additive form and \mathbf{U}_j only captures policy areas and positions.

We estimate the latent persuasiveness function $\mu(T_j, \mathbf{U}_j)$ using a neural network architecture and fine-tuning procedure similar to those employed in the previous applications. This approach allows us to evaluate the effect of each rhetorical element while adjusting for latent confounding features embedded in the arguments. To quantify uncertainty, we use Monte Carlo dropout (Gal and Ghahramani, 2016) during inference. Theoretical details and implementation specifics are provided in Appendix S3.

Figure 4 presents the estimated effects of the 14 rhetorical elements. We find that appeals to authority is the most persuasive. In contrast, ad hominem attacks—arguments targeting the person rather than their position—significantly reduce persuasiveness. These findings are consistent across

GenAI models and each model’s point estimates are highly correlated (see Appendix Figure S4). While these findings are largely consistent with those of the original analysis, the GPI estimates are substantially more precise despite the fact that the GPI does not impose parametric assumptions. For instance, the original results did not find statistically significant effects for appeals to authority or cost/benefit arguments, despite similar point estimates.

3 Concluding Remarks

In this paper, we introduced Generative AI-Powered Inference (GPI), a statistical framework that harnesses open-source generative AI models to improve causal and predictive inference with unstructured data, such as text and images. GPI extracts internal representations from these models, yielding low-dimensional features that preserve the all relevant information that are used to generate the data. By applying machine learning to these representations, GPI enables robust estimation of causal and predictive effects, while also quantifying estimation uncertainty. We demonstrated GPI’s broad applicability by revisiting and improving three published empirical studies.

This work opens several promising avenues for future research. First, developing methods to interpret the estimated deconfounders would help researchers better understand the latent confounding features identified by GPI. Second, GPI could be extended to discover effective treatment features from unstructured data. While the current framework assumes treatment features are predefined and observed, many applications would benefit from discovering novel, more informative treatments. Finally, although we focused on text and image data, the GPI framework can be naturally extended to other types of unstructured data, including audio and video.

References

- Ahrens, M., Ashwin, J., Calliess, J.-P., and Nguyen, V. (2021). Bayesian Topic Regression for Causal Inference. *arXiv:2109.05317 [cs, stat]*.
- Akiba, T., Sano, S., Yanase, T., Ohta, T., and Koyama, M. (2019). Optuna: A Next-generation Hyperparameter Optimization Framework. In *Proceedings of the 25th ACM SIGKDD International Conference on Knowledge Discovery & Data Mining*, KDD ’19, pages 2623–2631, New York, NY, USA. Association for Computing Machinery.
- Bach, P., Schacht, O., Chernozhukov, V., Klaassen, S., and Spindler, M. (2024). Hyperparameter tuning for causal inference with double machine learning: A simulation study. In *Causal Learning and Reasoning*, pages 1065–1117. PMLR.
- Bamman, D., O’Connor, B., and Smith, N. (2012). Censorship and deletion practices in chinese social media. *First Monday*.
- Barrie, C., Palmer, A., and Spirling, A. (2024). Replication for language models problems, principles, and best practice for political science. *Working Paper*.
- Blumenau, J. and Lauderdale, B. E. (2022). The Variable Persuasiveness of Political Rhetoric. *American Journal of Political Science*, n/a(n/a). eprint: <https://onlinelibrary.wiley.com/doi/pdf/10.1111/ajps.12703>.
- Bos, L., Van Der Brug, W., and De Vreese, C. H. (2013). An experimental test of the impact of style and rhetoric on the perception of right-wing populist and mainstream party leaders. *Acta Politica*, 48:192–208.

- Bradley, R. A. and Terry, M. E. (1952). Rank analysis of incomplete block designs: I. the method of paired comparisons. *Biometrika*, 39(3/4):324–345.
- Chernozhukov, V., Chetverikov, D., Demirer, M., Duflo, E., Hansen, C., Newey, W., and Robins, J. (2018). Double/debiased machine learning for treatment and structural parameters. *The Econometrics Journal*, 21(1):C1–C68.
- Christgau, A. M. and Hansen, N. R. (2024). Efficient adjustment for complex covariates: Gaining efficiency with dope. *arXiv preprint arXiv:2402.12980*.
- Daoud, A., Jerzak, C. T., and Johansson, R. (2022). Conceptualizing Treatment Leakage in Text-based Causal Inference. *arXiv:2205.00465 [cs]*.
- Dorn, J. (2025). How much weak overlap can doubly robust t-statistics handle?
- D’Amour, A., Ding, P., Feller, A., Lei, L., and Sekhon, J. (2021). Overlap in observational studies with high-dimensional covariates. *Journal of Econometrics*, 221(2):644–654.
- Egami, N., Fong, C. J., Grimmer, J., Roberts, M. E., and Stewart, B. M. (2022). How to make causal inferences using texts. *Science Advances*, 8(42):eabg2652. Publisher: American Association for the Advancement of Science.
- Farrell, M. H., Liang, T., and Misra, S. (2021). Deep Neural Networks for Estimation and Inference. *Econometrica*, 89(1):181–213. [eprint: https://onlinelibrary.wiley.com/doi/pdf/10.3982/ECTA16901](https://onlinelibrary.wiley.com/doi/pdf/10.3982/ECTA16901).
- Fong, C. and Grimmer, J. (2016). Discovery of Treatments from Text Corpora. In *Proceedings of the 54th Annual Meeting of the Association for Computational Linguistics (Volume 1: Long Papers)*, pages 1600–1609, Berlin, Germany. Association for Computational Linguistics.
- Fu, K.-w., Chan, C.-h., and Chau, M. (2013). Assessing censorship on microblogs in china: Discriminatory keyword analysis and the real-name registration policy. *IEEE internet computing*, 17(3):42–50.
- Gal, Y. and Ghahramani, Z. (2016). Dropout as a bayesian approximation: Representing model uncertainty in deep learning. In *international conference on machine learning*, pages 1050–1059. PMLR.
- Gouk, H., Frank, E., Pfahringer, B., and Cree, M. J. (2021). Regularisation of neural networks by enforcing lipschitz continuity. *Machine Learning*, 110:393–416.
- Grattafiori, A., Dubey, A., Jauhri, A., Pandey, A., Kadian, A., Al-Dahle, A., Letman, A., Mathur, A., Schelten, A., Vaughan, A., et al. (2024). The llama 3 herd of models. *arXiv preprint arXiv:2407.21783*.
- Gui, L. and Veitch, V. (2023). Causal Estimation for Text Data with (Apparent) Overlap Violations. *arXiv:2210.00079 [cs, stat]*.
- Iacus, S. M., King, G., and Porro, G. (2012). Causal inference without balance checking: Coarsened exact matching. *Political analysis*, 20(1):1–24.
- Imai, K. and Nakamura, K. (2024). Causal representation learning with generative artificial intelligence: Application to texts as treatments. *arXiv preprint arXiv:2410.00903*.

- Jerit, J. (2009). How predictive appeals affect policy opinions. *American Journal of Political Science*, 53(2):411–426.
- King, G., Pan, J., and Roberts, M. E. (2013). How Censorship in China Allows Government Criticism but Silences Collective Expression. *American Political Science Review*, 107(2):326–343.
- Klaassen, S., Teichert-Kluge, J., Bach, P., Chernozhukov, V., Spindler, M., and Vijaykumar, S. (2024). DoubleMLDeep: Estimation of Causal Effects with Multimodal Data. arXiv:2402.01785 [cs, econ, stat].
- Lindholm, A., Hjorth, C., and Schuessler, J. (2024). Facial finetuning: using pretrained image classification models to predict politicians’ success. *Political Science Research and Methods*, pages 1–11.
- Mesnard, T., Hardin, C., Dadashi, R., Bhupatiraju, S., Pathak, S., Sifre, L., Rivière, M., Kale, M. S., Love, J., Tafti, P., Hussenot, L., Sessa, P. G., Chowdhery, A., Roberts, A., Barua, A., Botev, A., Castro-Ros, A., Slone, A., Héliou, A., Tacchetti, A., Bulanov, A., Paterson, A., Tsai, B., Shahriari, B., Lan, C. L., Choquette-Choo, C. A., Crepy, C., Cer, D., Ippolito, D., Reid, D., Buchatskaya, E., Ni, E., Noland, E., Yan, G., Tucker, G., Muraru, G.-C., Rozhdestvenskiy, G., Michalewski, H., Tenney, I., Grishchenko, I., Austin, J., Keeling, J., Labanowski, J., Lespiau, J.-B., Stanway, J., Brennan, J., Chen, J., Ferret, J., Chiu, J., Mao-Jones, J., Lee, K., Yu, K., Millican, K., Sjoesund, L. L., Lee, L., Dixon, L., Reid, M., Mikula, M., Wirth, M., Sharman, M., Chinaev, N., Thain, N., Bachem, O., Chang, O., Wahltinez, O., Bailey, P., Michel, P., Yotov, P., Chaabouni, R., Comanescu, R., Jana, R., Anil, R., McIlroy, R., Liu, R., Mullins, R., Smith, S. L., Borgeaud, S., Girgin, S., Douglas, S., Pandya, S., Shakeri, S., De, S., Klimenko, T., Hennigan, T., Feinberg, V., Stokowiec, W., hui Chen, Y., Ahmed, Z., Gong, Z., Warkentin, T., Peran, L., Giang, M., Farabet, C., Vinyals, O., Dean, J., Kavukcuoglu, K., Hassabis, D., Ghahramani, Z., Eck, D., Barral, J., Pereira, F., Collins, E., Joulin, A., Fiedel, N., Senter, E., Andreev, A., and Kenealy, K. (2024). Gemma: Open models based on gemini research and technology.
- Mozer, R., Miratrix, L., Kaufman, A. R., and Anastasopoulos, L. J. (2020). Matching with Text Data: An Experimental Evaluation of Methods for Matching Documents and of Measuring Match Quality. *Political Analysis*, 28(4):445–468. Publisher: Cambridge University Press.
- Peterson, J. C., Uddenberg, S., Griffiths, T. L., Todorov, A., and Suchow, J. W. (2022). Deep models of superficial face judgments. *Proceedings of the National Academy of Sciences*, 119(17):e2115228119.
- Pryzant, R., Card, D., Jurafsky, D., Veitch, V., and Sridhar, D. (2021). Causal Effects of Linguistic Properties. arXiv:2010.12919 [cs].
- Roberts, M. E., Stewart, B. M., and Airolidi, E. M. (2016). A Model of Text for Experimentation in the Social Sciences. *Journal of the American Statistical Association*, 111(515):988–1003. Publisher: Taylor & Francis .eprint: <https://doi.org/10.1080/01621459.2016.1141684>.
- Roberts, M. E., Stewart, B. M., and Nielsen, R. A. (2020). Adjusting for Confounding with Text Matching. *American Journal of Political Science*, 64(4):887–903. .eprint: <https://onlinelibrary.wiley.com/doi/pdf/10.1111/ajps.12526>.
- Rombach, R., Blattmann, A., Lorenz, D., Esser, P., and Ommer, B. (2022). High-Resolution Image Synthesis With Latent Diffusion Models. pages 10684–10695.

- Rubin, D. B. (1990). Comments on “On the application of probability theory to agricultural experiments. Essay on principles. Section 9” by J. Splawa-Neyman translated from the Polish and edited by D. M. Dabrowska and T. P. Speed. *Statistical Science*, 5:472–480.
- Shalit, U., Johansson, F. D., and Sontag, D. (2017). Estimating individual treatment effect: generalization bounds and algorithms. arXiv:1606.03976 [cs, stat].
- Shi, C., Blei, D., and Veitch, V. (2019). Adapting Neural Networks for the Estimation of Treatment Effects. In *Advances in Neural Information Processing Systems*, volume 32. Curran Associates, Inc.
- Sutherland, C. A., Oldmeadow, J. A., Santos, I. M., Towler, J., Burt, D. M., and Young, A. W. (2013). Social inferences from faces: Ambient images generate a three-dimensional model. *Cognition*, 127(1):105–118.
- Todorov, A., Olivola, C. Y., Dotsch, R., and Mende-Siedlecki, P. (2015). Social attributions from faces: Determinants, consequences, accuracy, and functional significance. *Annual review of psychology*, 66(1):519–545.
- Tsiatis, A. A. (2006). *Semiparametric theory and missing data*. Springer series in statistics. Springer, New York, NY.
- Veitch, V., Sridhar, D., and Blei, D. M. (2020). Adapting Text Embeddings for Causal Inference. arXiv:1905.12741 [cs, stat].

Supplementary Materials

S1 Text as Confounder

In this section, we provide a formal theoretical justification of our methodology introduced in Section 2.1 and its implementation details.

S1.1 Theoretical Properties

Our approach extends the method proposed by Imai and Nakamura (2024) to the case of text as confounder. We begin by defining the causal quantity of interest. We then establish its nonparametric identification and develop an estimation strategy.

S1.1.1 Assumptions and Identification

Suppose we observe a sample of N independent and identically distributed (i.i.d.) units $i = 1, \dots, N$ from a population of interest. For each unit i , we observe a treatment assignment $T_i \in \mathcal{T} \subset \mathbb{R}$ and an observed outcome $Y_i \in \mathcal{Y} \subset \mathbb{R}$, where \mathcal{T} and \mathcal{Y} denote the support of the treatment and that of the outcome, respectively. Additionally, we observe a set of covariates $\mathbf{Z}_i \in \mathcal{Z} \subset \mathbb{R}^d$ and unstructured high-dimensional objects (e.g., texts or images) $\mathbf{X}_i \in \mathcal{X} \subset \mathbb{R}^r$, which also serve as confounders.

We adopt the potential outcomes framework for causal inference and assume the standard consistency assumption (Rubin, 1990). Specifically, we assume that the potential outcome, denoted by $Y_i(t)$, depends solely on the treatment assigned to unit i , not on the treatment assignments of other units. This is formalized as follows:

ASSUMPTION 1 (CONSISTENCY) *The potential outcome under the treatment $t \in \mathcal{T}$ is denoted by $Y_i(t)$, and equals to the observed outcome Y_i under the realized treatment assignment T_i :*

$$Y_i = Y_i(T_i)$$

We are interested in estimating the marginal distribution of the potential outcome under treatment condition $T_i = t$ for some $t \in \mathcal{T}$ (i.e., $\mathbb{P}(Y_i(t) = y)$). This can be used to estimate the average treatment effect (ATE) and other causal quantities of interest. We consider the strong latent ignorability assumption; conditional on the observed covariates and certain unknown features of the high-dimensional unstructured objects, potential outcomes are independent of treatment assignment.

ASSUMPTION 2 (STRONG LATENT IGNORABILITY WITH UNKNOWN CONFOUNDING FEATURES) *There exists a deterministic function $g_{\mathbf{U}} : \mathcal{X} \rightarrow \mathcal{U}$ that maps an unstructured object \mathbf{X}_i on to the low-dimensional confounding features $\mathbf{U}_i \in \mathcal{U}$ with $\dim(\mathbf{U}) \ll \dim(\mathbf{X})$ such that the potential outcomes are independent of the treatment assignment given the observed covariates \mathbf{Z}_i and the confounding features $\mathbf{U}_i = g_{\mathbf{U}}(\mathbf{X}_i)$:*

$$\{Y_i(t)\}_{t \in \mathcal{T}} \perp\!\!\!\perp T_i \mid \mathbf{Z}_i = \mathbf{z}, \mathbf{U}_i = \mathbf{u},$$

where $\mathbb{P}(T_i = t \mid \mathbf{Z}_i = \mathbf{z}, \mathbf{U}_i = \mathbf{u}) > 0$ for all $t \in \mathcal{T}$, $\mathbf{z} \in \mathcal{Z}$, and $\mathbf{u} \in \mathcal{U}$.

Importantly, we assume the existence of low-dimensional features \mathbf{U}_i , which are deterministic functions of the unstructured objects and sufficient to satisfy the strong ignorability assumption. We do not condition directly on the high-dimensional unstructured objects \mathbf{X}_i , as such data (e.g., texts or images) can often perfectly predict treatment assignment, thereby violating the positivity

condition and inducing significant bias in estimates (D’Amour et al., 2021). Prior work either overlooks this issue (e.g., Veitch et al. 2020; Klaassen et al. 2024) or addresses it by using text-based matching (e.g., Roberts et al. 2020; Mozer et al. 2020). Matching is not well suited for high-dimensional controls and the reliance on parametric propensity score models such as topic models leads to bias. In contrast, our method assumes only the existence of low-dimensional confounding features \mathbf{U}_i .

Finally, we assume that unstructured objects are generated by a deep generative model. When the existing image and text are of interest, we can regenerate them by appropriately prompting a deep generative model. Following Imai and Nakamura (2024), we adopt a broad definition of deep generative model to encompass LLMs and other foundation models.

DEFINITION 1 (DEEP GENERATIVE MODEL) *A deep generative model is the following probabilistic model that takes prompt \mathbf{P}_i as an input and generates the unstructured object \mathbf{X}_i as an output:*

$$\begin{aligned} \mathbb{P}(\mathbf{X}_i \mid \mathbf{h}_\gamma(\mathbf{R}_i)) \\ \mathbb{P}(\mathbf{R}_i \mid \mathbf{P}_i) \end{aligned}$$

where $\mathbf{R}_i \in \mathcal{R} \subset \mathbb{R}^d$ denotes an internal representation of \mathbf{X}_i contained in the model and $\mathbf{h}_\gamma(\mathbf{R}_i)$ is a deterministic function parameterized by γ that completely characterizes the conditional distribution of \mathbf{X}_i given \mathbf{R}_i .

Under this definition of deep generative model, \mathbf{R} represents a lower-dimensional representation of the unstructured object \mathbf{X} and is a hidden representation of neural networks. We assume that the last layer of the deep generative model is a deterministic function of the internal representation \mathbf{R}_i so that the low-dimensional features of the unstructured object \mathbf{U}_i can be regarded as a deterministic function of the low-dimensional internal representation \mathbf{R}_i of the deep generative model.

ASSUMPTION 3 (DETERMINISTIC DECODING) *The output layer of a deep generative model is deterministic. That is, $\mathbb{P}(\mathbf{X}_i \mid \mathbf{h}_\gamma(\mathbf{R}_i))$ in Definition 1 is a degenerate distribution.*

Importantly, we only require that \mathbf{R}_i deterministically generates the unstructured object \mathbf{X}_i . For example, some generative models, especially diffusion models, have an internal architecture that is stochastic, but the output of the decoder layer can be made deterministic so that GPI is still applicable. In the case of LLMs, Barrie et al. (2024) shows that due to updates to the internal parameters, the outputs of LLMs are not generally replicable over time. However, in this context, we are only concerned with the deterministic relationship between \mathbf{R}_i and \mathbf{X}_i , which can be controlled by selecting appropriate hyperparameters for any given LLM.

Figure S1 presents a directed acyclic graph (DAG) that summarizes the data generating process and assumptions described above. In this DAG, an arrow with double red-colored lines represents a deterministic causal relation while an arrow with a single line represents a stochastic causal relation. The dashed line bidirectional arrow represents the potential independence relation.

Given this setup, we establish the nonparametric identification of the marginal distribution of the potential outcome under the treatment condition $T_i = t$ for any given $t \in \mathcal{T}$. We extend the results of Imai and Nakamura (2024) to the case of unstructured objects as confounder, accommodating potentially non-binary treatments and observed structured confounders.

We show that there exists a deconfounder function $\mathbf{f}(\mathbf{R}_i)$ satisfying the conditional independence relation $Y_i \perp\!\!\!\perp \mathbf{R}_i \mid T_i, \mathbf{Z}_i, \mathbf{f}(\mathbf{R}_i)$, where $\mathbf{f}(\mathbf{R}_i)$ is a deterministic function of the internal representation \mathbf{R}_i . The existence of such a function is guaranteed by Assumptions 2 and 3, since \mathbf{U}_i is a deterministic function of \mathbf{R}_i and satisfies the conditional independence condition. Moreover,

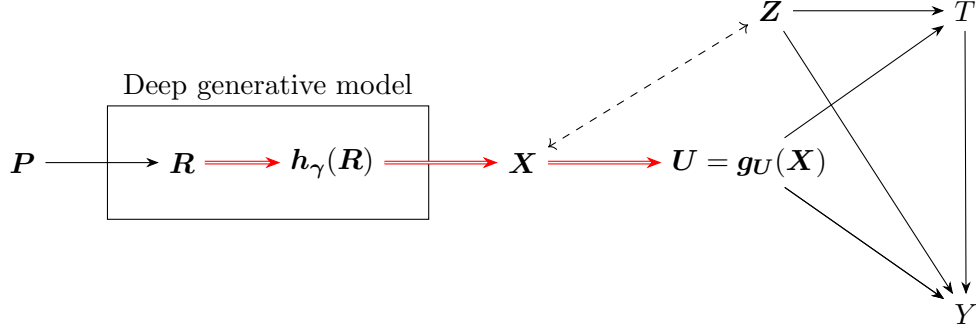


Figure S1: Directed Acyclic Graph of the Assumed Data-Generating Process with an Unstructured Confounder. An unstructured object \mathbf{X} (e.g., an image or text) is generated via a deep generative model (shown as a rectangle), where a prompt \mathbf{P} produces an internal representation \mathbf{R} , which is then transformed into \mathbf{X} by the function $h_\gamma(\mathbf{R})$. The causal relationship between treatment T and outcome Y is confounded by both observed structured covariates \mathbf{Z} and latent confounding features \mathbf{U} embedded within the unstructured object \mathbf{X} . Arrows with red double lines represent deterministic causal relationships; single-lined arrows denote possibly stochastic relationships; and dashed bidirectional arrows indicate potential independence.

any deconfounder function that satisfies the conditional independence relation leads to the same identification formula.

PROPOSITION 1 (NONPARAMETRIC IDENTIFICATION) *Under Assumptions 1 and 2, there exists a deconfounder function $\mathbf{f} : \mathbb{R}^r \mapsto \mathbb{R}^q$ with $q \leq r$ that satisfies the following independence relation:*

$$Y_i \perp\!\!\!\perp \mathbf{R}_i \mid T_i, \mathbf{Z}_i, \mathbf{f}(\mathbf{R}_i).$$

By adjusting this deconfounder, we can nonparametrically identify the marginal distribution of the potential outcome under the treatment condition $T_i = t$ as,

$$\mathbb{P}(Y_i(t) = y) = \int_{\mathbb{R}^q} \int_{\mathcal{Z}} \mathbb{P}(Y_i = y \mid T_i = t, \mathbf{Z}_i, \mathbf{f}(\mathbf{R}_i)) dF(\mathbf{Z}_i) dF(\mathbf{R}_i) \quad (\text{S1})$$

where $y \in \mathcal{Y}$.

See Section S4 for the proof.

S1.1.2 Estimation and Inference

Given the identification formula, we now turn to estimation and statistical inference. We extend the estimation procedure of Imai and Nakamura (2024) to the current setting. Our strategy relies on two key observations. First, Assumption 2 implies that the deconfounder is not a post-treatment variable. Second, the deconfounder must satisfy the conditional independence condition stated in Equation (S1).

We use a neural network architecture that extends TarNet (Shalit et al., 2017) to non-binary treatment and structured confounding variables to estimate the conditional potential outcome function given the deconfounder and observed control variables, i.e.,

$$\mu_{T_i}(\mathbf{f}(\mathbf{R}_i), \mathbf{Z}_i) = \mathbb{E}[Y_i(t) \mid \mathbf{f}(\mathbf{R}_i), \mathbf{Z}_i]$$

Our proposed neural network architecture, which is summarized in Figure S2, simultaneously estimates the deconfounder $\mathbf{f}(\mathbf{R}_i)$ and the conditional potential outcome function $\mu_{T_i}(\mathbf{f}(\mathbf{R}_i), \mathbf{Z}_i) :=$

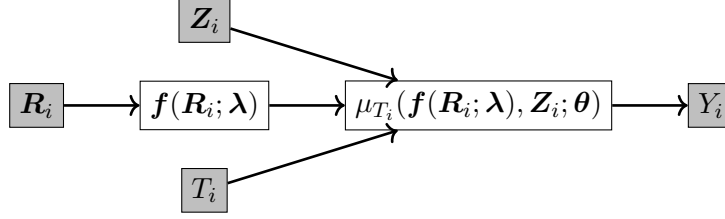


Figure S2: Diagram Illustrating the Proposed Model Architecture when Unstructured Object is Confounder. The proposed model takes an internal representation of unstructured object \mathbf{R}_i as an input, and finds a deconfounder $\mathbf{f}(\mathbf{R}_i)$, which is a lower-dimensional representation of \mathbf{R}_i , and then use it together with the treatment T_i and structured confounder \mathbf{Z}_i to predict the conditional expectation of the outcome $\mu_{T_i}(\mathbf{f}(\mathbf{R}_i), \mathbf{Z}_i) := \mathbb{E}[Y_i \mid T_i, \mathbf{f}(\mathbf{R}_i), \mathbf{Z}_i]$. The architecture encodes the conditional independence relation $Y_i \perp\!\!\!\perp \mathbf{R}_i \mid T_i, \mathbf{Z}_i, \mathbf{f}(\mathbf{R}_i)$.

$\mathbb{E}[Y_i \mid T_i, \mathbf{f}(\mathbf{R}), \mathbf{Z}_i]$, by first projecting the internal representation \mathbf{R}_i onto a lower dimensional space of deconfounder \mathbf{f} . We then use the estimated deconfounder, treatment vector T_i , and observed structured confounders \mathbf{Z}_i , we predict the conditional potential outcome function μ_{T_i} by minimizing the following loss function:

$$\{\hat{\boldsymbol{\lambda}}, \hat{\boldsymbol{\theta}}\} = \underset{\boldsymbol{\lambda}, \boldsymbol{\theta}}{\operatorname{argmin}} \frac{1}{N} \sum_{i=1}^N \{Y_i - \mu_{T_i}(\mathbf{f}(\mathbf{R}_i; \boldsymbol{\lambda}), \mathbf{Z}_i; \boldsymbol{\theta})\}^2, \quad (\text{S2})$$

where $\boldsymbol{\lambda}$ is the parameter of the deconfounder function $\mathbf{f}(\mathbf{R}_i)$, and $\boldsymbol{\theta}$ is the parameter of the conditional potential outcome function $\mu(\mathbf{f}(\mathbf{R}_i), T_i, \mathbf{Z}_i; \boldsymbol{\theta})$.

Importantly, our method is different from the existing methods of causal inference for texts because we do not predict treatment assignment given the internal representation. The joint estimation of treatment assignment and outcome models, as done in the methods like DragonNet (Shi et al., 2019), leads to $\mathbb{P}(T_i = 1 \mid \mathbf{f}(\mathbf{R}_i), \mathbf{Z}_i) = \mathbb{P}(T_i = 1 \mid \mathbf{R}_i, \mathbf{Z}_i)$. As a result, these methods are likely to violate the positivity assumption. The recent literature on causal representation learning demonstrates that we can achieve the efficient estimation by combining the internal low-dimensional representation and propensity score models (Christgau and Hansen 2024).

Given the proposed neural network architecture, we estimate the Average Treatment Effect for the Treated (ATT) using double machine learning (DML) (Chernozhukov et al., 2018). We estimate ATT to compare our result with the original analysis based on text matching. Here, we propose to estimate the propensity score model as a function of the estimated deconfounder, i.e., $\pi_t(\mathbf{f}(\mathbf{R}_i), \mathbf{Z}_i) = \mathbb{P}(T_i = t \mid \mathbf{f}(\mathbf{R}_i), \mathbf{Z}_i)$ so that we do not directly condition on the high-dimensional unstructured objects.

To ensure the asymptotic normality discussed later in this section, the propensity score model must be Lipschitz-continuous; accordingly, we employ a neural network with spectral normalization (Gouk et al., 2021). Practical implementation requires careful tuning of the hyperparameters for both the outcome and propensity score models, including network width and depth, learning rate, batch size, dropout rate, and number of epochs. We automate this with advanced hyperparameter-optimization tools such as Optuna (Akiba et al., 2019).

As an example, we present the entire estimation procedure in the case of binary treatment $\mathcal{T} = \{0, 1\}$. Denote the observed data by $\mathcal{D} := \{\mathcal{D}_i\}_{i=1}^N$ where $\mathcal{D}_i := \{Y_i, T_i, \mathbf{R}_i, \mathbf{Z}_i\}$. We use the following K -fold cross-fitting procedure, assuming that N is divisible by K .

1. Randomly partition the data into K folds of equal size where the size of each fold is $n = N/K$.

The observation index is denoted by $I(i) \in \{1, \dots, K\}$ where $I(i) = k$ implies that the i th observation belongs to the k th fold.

2. For each fold $k \in \{1, \dots, K\}$, use observations with $I(i) \neq k$ as training data:

- (a) further split the training data into two folds, $I_1^{(-k)}$ and $I_2^{(-k)}$
- (b) simultaneously obtain an estimated deconfounder and an estimated conditional outcome function on the first fold, which are denoted by $\hat{\mathbf{f}}^{(-k)}(\{\mathbf{R}_i, \mathbf{Z}_i\}_{i \in I_1^{(-k)}}) := \mathbf{f}(\{\mathbf{R}_i, \mathbf{Z}_i\}_{i \in I_1^{(-k)}}; \hat{\boldsymbol{\lambda}}^{(-k)})$ and $\hat{\mu}_t^{(-k)}(\{\mathbf{R}_i, \mathbf{Z}_i\}_{i \in I_1^{(-k)}}) := \mu_t(\mathbf{f}(\{\mathbf{R}_i\}_{i \in I_1^{(-k)}}; \hat{\boldsymbol{\lambda}}^{(-k)}), \mathbf{Z}_i; \hat{\boldsymbol{\theta}}^{(-k)})$, respectively, by solving the optimization problem given in Equation (S2), and
- (c) obtain an estimated propensity score given the estimated deconfounder on the second fold, which is denoted by $\hat{\pi}^{(-k)}(\hat{\mathbf{f}}^{(-k)}(\{\mathbf{R}_i\}_{i \in I_2^{(-k)}}), \mathbf{Z}_i) := \hat{\pi}^{(-k)}(\mathbf{f}(\{\mathbf{R}_i\}_{i \in I_2^{(-k)}}; \hat{\boldsymbol{\lambda}}^{(-k)}), \mathbf{Z}_i)$.

3. Compute the ATT estimator $\hat{\tau}$ as a solution to:

$$\frac{1}{nK} \sum_{k=1}^K \sum_{i: I(i)=k} \psi(\mathcal{D}_i; \hat{\tau}, \hat{\mathbf{f}}^{(-k)}, \mu_0^{(-k)}, \hat{\pi}^{(-k)}) = 0,$$

where

$$\begin{aligned} & \psi(\mathcal{D}_i; \tau, \mathbf{f}, \mu_0, \pi) \\ &= \frac{T_i(Y_i - \mu_0(\mathbf{f}(\mathbf{R}_i), \mathbf{Z}_i))}{\mathbb{P}(T_i = 1)} - \frac{\pi(\mathbf{f}(\mathbf{R}_i), \mathbf{Z}_i)(1 - T_i)(Y_i - \mu_0(\mathbf{f}(\mathbf{R}_i), \mathbf{Z}_i))}{\mathbb{P}(T_i = 1)(1 - \pi(\mathbf{f}(\mathbf{R}_i), \mathbf{Z}_i))} - \frac{T_i \tau}{\mathbb{P}(T_i = 1)}. \end{aligned} \quad (\text{S3})$$

Finally, we establish the asymptotic properties of the proposed estimator in the case of binary treatment. We assume that the following regularity conditions hold. These conditions are similar to those in Imai and Nakamura (2024) except that we also condition on the observed covariates \mathbf{Z}_i .

ASSUMPTION 4 (REGULARITY CONDITIONS) *Let c_1 , c_2 , and $q > 2$ be positive constants and δ_n be a sequence of positive constants approaching zero as the sample size n increases. Then, the following conditions hold.*

(a) *(Primitive conditions)*

$$\begin{aligned} \mathbb{E}[|Y_i|^q]^{1/q} &\leq c_1, \quad \sup_{\mathbf{r} \in \mathcal{R}, \mathbf{z} \in \mathcal{Z}} \mathbb{E}[|Y_i - \mu_{T_i}(\mathbf{f}(\mathbf{r}), \mathbf{z})|^2 \mid \mathbf{R}_i = \mathbf{r}, \mathbf{Z}_i = \mathbf{z}] \leq c_1, \\ \mathbb{E}[|Y_i - \mu_{T_i}(\mathbf{f}(\mathbf{R}_i), \mathbf{Z}_i)|^2]^{1/2} &\geq c_2. \end{aligned}$$

(b) *(Outcome model estimation)*

$$\mathbb{E}[|\hat{\mu}_{T_i}(\hat{\mathbf{f}}(\mathbf{R}_i), \mathbf{Z}_i) - \mu_{T_i}(\mathbf{f}(\mathbf{R}_i), \mathbf{Z}_i)|^q]^{1/q} \leq c_1, \quad \mathbb{E}[|\hat{\mu}_{T_i}(\hat{\mathbf{f}}(\mathbf{R}_i), \mathbf{Z}_i) - \mu_{T_i}(\mathbf{f}(\mathbf{R}_i), \mathbf{Z}_i)|^2]^{1/2} \leq \delta_n n^{-1/4}.$$

(c) *(Deconfounder estimation)*

$$\mathbb{E} \left[\left\| \hat{\mathbf{f}}(\mathbf{R}_i) - \mathbf{f}(\mathbf{R}_i) \right\|^q \right]^{1/q} \leq c_1, \quad \mathbb{E} \left[\left\| \hat{\mathbf{f}}(\mathbf{R}_i) - \mathbf{f}(\mathbf{R}_i) \right\|^2 \right]^{1/2} \leq \delta_n n^{-1/4}$$

(d) *(Propensity score estimation) $\pi(\cdot)$ is Lipschitz continuous at the every point of its support, and satisfies:*

$$\mathbb{E}[|\hat{\pi}(\mathbf{f}(\mathbf{R}_i), \mathbf{Z}_i) - \pi(\mathbf{f}(\mathbf{R}_i), \mathbf{Z}_i)|^q]^{1/q} \leq c_1, \quad \mathbb{E}[|\hat{\pi}(\mathbf{f}(\mathbf{R}_i), \mathbf{Z}_i) - \pi(\mathbf{f}(\mathbf{R}_i), \mathbf{Z}_i)|^2]^{1/2} \leq \delta_n n^{-1/4}.$$

These regularity conditions are standard in the DML literature, and it is known that the neural network architecture with an appropriate depth and width can achieve the required convergence rates (Farrell et al., 2021). The propensity score requires the Lipschitz continuity condition, which can be satisfied by using a regularized neural network architecture (Gouk et al., 2021).

Given the above assumptions, the asymptotic normality of the proposed estimator follows immediately from the DML theory.

THEOREM 1 (ASYMPTOTIC NORMALITY OF THE ATT ESTIMATOR) *Under Assumptions 1–4, the estimator $\hat{\tau}$ obtained from the influence function ψ satisfies asymptotic normality:*

$$\frac{\sqrt{n}(\hat{\tau} - \tau)}{\sigma} \xrightarrow{d} \mathcal{N}(0, 1)$$

where $\sigma^2 = \mathbb{E}[\psi(\mathcal{D}_i; \tau, \mathbf{f}, \mu_1, \mu_0, \pi_1)^2]$.

We omit the proof as it is identical to Theorem 1 of Imai and Nakamura (2024).

S1.2 Implementation Details for the Empirical Application

We reanalyze the dataset used by Roberts et al. (2020), which is based on data from the Weiboscope project (Fu et al., 2013). This project collected Weibo posts in real time and subsequently revisited them to determine whether they had been censored. The original analysis focused on users who experienced at least one instance of censorship during the first half of 2012, and examined their subsequent posts in the second half of that year. To construct the control group, the authors selected posts that had a cosine similarity greater than 0.5 to a censored post and were posted on the same day. Posts shorter than 15 characters were excluded. The final dataset we analyze consists of 75,324 posts from 4,155 Weibo users.

Based on the treatment and control “focal” posts, three outcome variables were constructed:

1. The number of posts made by the same user within the four weeks following the focal post
2. The proportion of those posts that were censored (as indicated by a “permission denied” message)
3. The proportion of posts that went missing (as indicated by a “Weibo does not exist” message)

It is important to note that the second and third outcomes capture different types of post removals. As noted by Fu et al. (2013), a “permission denied” message is a clear signal of censorship, whereas “Weibo does not exist” may reflect either censorship or voluntary deletion by the user. To adjust for users’ baseline behavior, the same three measures were also computed for the four-week period preceding each focal post and included as confounding variables.

We apply the GPI methodology as follows. First, we use LLaMA 3 (8 billion parameters) and Gemma 3 (1 billion parameters) to regenerate all posts in the dataset and extract the internal representation of the last token. Due to the autoregressive nature of generative models, this final-token representation captures the full information of each post. The resulting internal representation, denoted by \mathbf{R}_i , has a dimensionality of 4096 for LLaMA3 and 1152 for Gemma3. Using this representation, we estimate the deconfounder $\mathbf{f}(\mathbf{R}_i)$ and the outcome model $\mu_{T_i}(\mathbf{f}(\mathbf{R}_i), \mathbf{Z}_i)$ via a neural network architecture described in the previous section.

To train the model for each outcome variable, we employed two-fold cross-validation on the full sample, following the recommendation of Bach et al. (2024). The hyperparameter search space included:

Model	Outcome	Learning Rate	Dropout	Outcome Model	Deconfounder
LLaMA3 (8B)	Number of Posts	1.188×10^{-7}	0.051	[100, 1]	[1024, 512]
	Rate of Censorship	9.974×10^{-5}	0.161	[100, 1]	[1024, 512]
	Rate of Missing Posts	9.858×10^{-5}	0.118	[50, 1]	[1024, 512]
Gemma3 (1B)	Number of Posts	2.726×10^{-7}	0.094	[100, 1]	[1024, 512]
	Rate of Censorship	7.678×10^{-5}	0.276	[50, 1]	[1024, 512]
	Rate of Missing Posts	7.499×10^{-5}	0.154	[50, 1]	[512, 256]

Table S1: Optimal hyperparameters selected for each outcome measure using Optuna. The table lists the learning rate, dropout rate, outcome model architecture, and deconfounder architecture applied to the reanalysis of Roberts et al. (2020).

- Learning rate: 10^{-7} to 10^{-4}
- Dropout rate: 0.05 to 0.3
- Outcome model architecture: single-layer MLP with ReLU activation and 50, 100, or 200 hidden units
- Deconfounder architecture: two-layer MLP with ReLU activation and hidden unit configurations of [256, 128], [512, 256], or [1024, 512]

We automated hyperparameter optimization using Optuna (Akiba et al., 2019), selecting the best parameters based on validation loss across 100 trials. For both hyperparameter tuning and nuisance function estimation, models were trained for up to 10000 epochs, with early stopping triggered if validation loss failed to improve for 5 consecutive epochs. We used the Adam optimizer with a batch size of 256 and a weight decay of 10^{-8} to prevent overfitting. To stabilize training, we applied gradient clipping with a maximum norm of 1.0. The optimal hyperparameter configurations for each outcome measure are reported in Table S1.

After selecting the optimal hyperparameters, we estimated the Average Treatment Effect for the Treated (ATT) for each outcome using the Double Machine Learning (DML) procedure described in the previous section. Specifically, we implemented 2-fold cross-fitting to estimate the nuisance components: the deconfounder $\mathbf{f}(\mathbf{R}_i)$, the outcome model $\mu_{T_i}(\mathbf{f}(\mathbf{R}_i), \mathbf{Z}_i)$, and the propensity score $\pi(\mathbf{f}(\mathbf{R}_i), \mathbf{Z}_i)$.

The deconfounder and outcome model were trained using the selected hyperparameters for up to 10000 epochs, with early stopping triggered if the validation loss did not improve for five consecutive epochs. For propensity score estimation, we used a neural network with spectral normalization (Gouk et al., 2021) to enforce Lipschitz continuity. This network consisted of a two-layer MLP with ReLU activation, using 128 hidden units in the first layer and 64 in the second. The learning rate was fixed at 10^{-5} , and the model was trained under the same early stopping criteria.

ATT was then computed using Equation (3), with standard errors derived from the influence function in Equation (S3). To account for within-user correlation, we clustered standard errors at the user level. For consistency with the original study’s text matching approach, we estimated the ATT using both the full sample and the matched sample from the original analysis.

For comparison, we replicated the text matching procedure proposed by Roberts et al. (2020), following their publicly available replication materials. Specifically, we fit a structural topic model

with 100 topics, incorporating the censorship indicator (treatment) as a covariate. From this model, we obtained both the estimated topic proportions and treatment projections for each post.

Next, we applied coarsened exact matching (CEM) to pair censored posts with uncensored ones based on four criteria: (1) topic proportions, (2) treatment projection, (3) post date, and (4) prior censorship history. This matching procedure yielded a final sample of 879 posts from 628 users. Using the matched sample and weights generated by CEM, we compared treatment and control posts across the three outcome measures described earlier. As in the main analysis, standard errors were clustered at the user level to account for within-user correlation.

To further assess the robustness of our approach, we examine the correlation between the estimated efficient scores of GPI and a potential confounding variable: the proportion of censorship-related keywords in each post. The literature of semiparametric statistics suggests that the estimated efficient score is mean independent of any observed confounder (e.g., Tsiatis, 2006). Thus, if the proposed method captures the confounding features in focal posts well, we expect the estimated efficient scores to be uncorrelated with this candidate confounder.

Specifically, we use a set of 60 keywords identified by Fu et al. (2013): (1) 30 keywords with the highest relative frequency in censored posts compared to uncensored ones, and (2) 30 keywords most frequent among self-censoring users relative to others (as reported in Appendix Tables 1a and 1b of Fu et al. 2013). Then, our candidate confounder is the proportion of these keywords in each post.

For GPI, we directly use the estimated efficient scores from the DML procedure and compute its Pearson’s correlation with the candidate confounder. For text matching, we compute the correlation between the candidate confounder and the residual from its implied weighted OLS (with weights from coarsened exact matching), which is proportional to the efficient score of the weighted OLS model. Finally, we cluster standard errors at the user level to account for within-user dependence.

S2 Predictive Effects of Image Features

In this section, we provide a formal theoretical justification of our methodology introduced in Section 2.2 and its implementation details.

S2.1 Theoretical Properties

While, strictly speaking, we are interested in predictive effects (i.e., difference in predicted outcome when a predictor of interest takes different values while holding other variables at their observed values) rather than causal effects, below we consider the identification and estimation of the latter, which requires more stringent assumptions. It is worth noting that estimated predictive effects remain valid even when they cannot be interpreted as causal effects due to the violation of additional assumptions.

Our identification results are nearly identical to the those of Imai and Nakamura (2024), with the key difference that we focus on images rather than texts, and additionally incorporate observed structured confounding variables. For estimation and inference, however, we extend their methodology to accommodate a multi-valued treatment. As in the previous section, we define the causal estimand of interest, establish its nonparametric identification, and then develop an appropriate estimation strategy.

S2.1.1 Assumptions and Identification

Suppose we observe a sample of N i.i.d. units $i = 1, \dots, N$ from a population of interest. For each unit i , we observe an unstructured treatment object $\mathbf{X}_i \in \mathcal{X} \subset \mathbb{R}^r$ (e.g., images or texts) and an observed outcome $Y_i \in \mathcal{Y} \subset \mathbb{R}$. Additionally, we observe a set of structured confounding variables $\mathbf{Z}_i \in \mathcal{Z} \subset \mathbb{R}^d$. As in the previous section, we assume that the treatment object \mathbf{X}_i is generated

by a deep generative model defined in Definition 1 and that the last layer of the deep generative model is a deterministic function of the internal representation \mathbf{R}_i (Assumption 3).

As before, we adopt the potential outcome framework. We denote the potential outcome under the treatment object $\mathbf{x} \in \mathcal{X}$ by $Y_i(\mathbf{x})$, which is defined as the outcome that would be observed if unit i were to receive treatment object \mathbf{x} . The observed outcome is denoted by Y_i and is defined as the potential outcome under the realized treatment object \mathbf{X}_i , i.e., $Y_i = Y_i(\mathbf{X}_i)$. This notation assumes no interference between units and no hidden multiple version of treatment objects (Rubin, 1990). This is formalized as follows:

ASSUMPTION 5 (CONSISTENCY) *The potential outcome under the treatment object $\mathbf{x} \in \mathcal{X}$ is denoted by $Y_i(\mathbf{x})$ and equals the observed outcome Y_i under the realized treatment object \mathbf{X}_i :*

$$Y_i = Y_i(\mathbf{X}_i).$$

As we are working in the observational studies setting without randomization, we rely on the standard ignorability assumption for causal identification. Specifically, we assume that given the observed covariates \mathbf{Z}_i , the assignment of the treatment object is independent of the potential outcomes. This is formalized as follows:

ASSUMPTION 6 (STRONG IGNORABILITY) *Conditional on the observed covariates \mathbf{Z}_i , the assignment of treatment object \mathbf{X} is independent of potential outcomes,*

$$Y_i(\mathbf{x}) \perp\!\!\!\perp \mathbf{X}_i \mid \mathbf{Z}_i = \mathbf{z},$$

where $0 < \mathbb{P}(\mathbf{X}_i = \mathbf{x} \mid \mathbf{Z}_i = \mathbf{z}) < 1$ for all $i = 1, \dots, N$, $\mathbf{x} \in \mathcal{X}$, and $\mathbf{z} \in \mathcal{Z}$.

We are interested in estimating the causal effect of a particular feature that can be part of a treatment object. We assume that the treatment feature T is determined solely by the treatment object \mathbf{X} .

ASSUMPTION 7 (TREATMENT FEATURE) *There exists a deterministic function $g_T : \mathcal{X} \rightarrow \mathcal{T}$ that maps a treatment object \mathbf{X}_i to a treatment feature of interest $T_i \in \mathcal{T}$, i.e.,*

$$T_i = g_T(\mathbf{X}_i).$$

The assumption implies that the treatment variable is a function of the treatment object and does not vary across respondents.

Next, we define confounding features, which represent all features of \mathbf{X} other than the treatment feature T that influence the outcome Y . These confounding features, denoted by \mathbf{U}_i , are based on a vector-valued deterministic function of \mathbf{X} and are denoted by $\mathbf{U} \in \mathcal{U}$ where \mathcal{U} denotes their support. As in the previous section, however, this confounding feature is not observed.

ASSUMPTION 8 (CONFOUNDING FEATURES) *There exists an unknown vector-valued deterministic function $g_U : \mathcal{X} \rightarrow \mathcal{U}$ that maps an unstructured object $\mathbf{X}_i \in \mathcal{X}$ to the confounding features $\mathbf{U}_i \in \mathcal{U}$, i.e.,*

$$\mathbf{U}_i = g_U(\mathbf{X}_i),$$

where $\dim(\mathbf{U}_i) \ll \dim(\mathbf{X}_i)$.

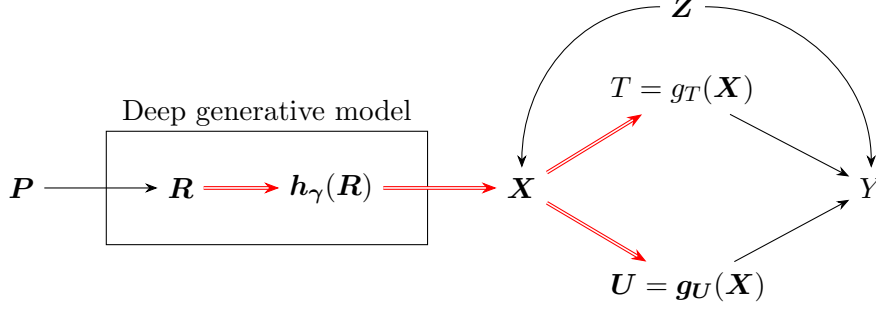


Figure S3: Directed Acyclic Graph of the Assumed Data Generating Process when the Treatment is an Unstructured Object. A treatment object \mathbf{X} (e.g., image) is generated using a deep generative model (rectangle) with a prompt \mathbf{P} , producing an internal representation \mathbf{R} that generates \mathbf{X} through a deterministic function $h_\gamma(\mathbf{R})$. The treatment object affects the outcome Y through its treatment feature of interest T and other confounding features U . Treatment object is assumed to be conditionally independent of potential outcomes given the observed structured confounding variables \mathbf{Z} . An arrow with red double lines represents a deterministic causal relation while an arrow with a single line indicates a possibly stochastic relationship.

Finally, we describe our key identification assumption that we can intervene the treatment feature without changing the confounding features. Specifically, we assume that the treatment feature cannot be represented as a deterministic function of the confounding features. In addition, confounding features should not be any function of treatment feature either because we only wish to adjust for pretreatment variables (Daoud et al., 2022). We formalize this assumption as follows.

ASSUMPTION 9 (SEPARABILITY OF TREATMENT AND CONFOUNDING FEATURES) *The potential outcome is a function of the treatment feature of interest t and another separate function of the confounding features \mathbf{u} . Specifically, for any given $\mathbf{x} \in \mathcal{X}$ and all i , we have:*

$$Y_i(\mathbf{x}) = Y_i(t, \mathbf{u}) = Y_i(g_T(\mathbf{x}), \mathbf{g}_U(\mathbf{x})),$$

where $t = g_T(\mathbf{x}) \in \mathcal{T}$ and $\mathbf{u} = \mathbf{g}_U(\mathbf{x}) \in \mathcal{U}$. In addition, g_T and \mathbf{g}_U are separable. That is, there exists no deterministic function $\tilde{g}_T : \mathcal{U} \rightarrow \mathcal{T}$, which satisfies $g_T(\mathbf{x}) = \tilde{g}_T(\mathbf{g}_U(\mathbf{x}))$ for all $\mathbf{x} \in \mathcal{X}$. Similarly, there exist no deterministic functions $\mathbf{g}' : \mathcal{X} \rightarrow \mathcal{X}'$ and $\tilde{\mathbf{g}}_U : \mathcal{T} \times \mathcal{X}' \rightarrow \mathcal{U}$, which satisfy $\mathbf{g}_U(\mathbf{x}) = \tilde{\mathbf{g}}_U(g_T(\mathbf{x}), \mathbf{g}'(\mathbf{x}))$ for all $\mathbf{x} \in \mathcal{X}$ and $\tilde{\mathbf{g}}_U(t, \mathbf{g}'(\mathbf{x}')) \neq \tilde{\mathbf{g}}_U(t', \mathbf{g}'(\mathbf{x}'))$ for $t \neq t'$ with $t, t' \in \mathcal{T}$ and some $\mathbf{x}' \in \mathcal{X}$.

Under this setup, we are interested in estimating the average potential outcome of the treatment feature while controlling for the confounding features, which is defined as follows:

$$\xi_t := \mathbb{E}[Y_i(t, \mathbf{U}_i)]. \quad (\text{S4})$$

Figure S3 presents a DAG that summarizes the data generating process and required assumptions for identification (Assumptions 3, and 5–9). As in the previous DAG, an arrow with double lines represents a deterministic causal relationship, while an arrow with a single line indicates a possibly stochastic causal relationship.

Given this setup, we establish the nonparametric identification of the dose-response curve defined in Equation (S4).

PROPOSITION 2 (NONPARAMETRIC IDENTIFICATION OF THE MARGINAL DISTRIBUTION OF POTENTIAL OUTCOME) *Under Assumptions 3, 5–9, there exists a deconfounder function $\mathbf{f} : \mathcal{R} \rightarrow \mathcal{Q} \subset \mathbb{R}^{d_Q}$ with $d_Q = \dim(\mathcal{Q}) \leq d_R = \dim(\mathcal{R})$ that satisfies the following conditional independence relation:*

$$Y_i \perp\!\!\!\perp \mathbf{R}_i \mid T_i = t, \mathbf{f}(\mathbf{R}_i) = \mathbf{q}, \mathbf{Z}_i \quad (\text{S5})$$

where $0 < \mathbb{P}(T_i = t \mid \mathbf{f}(\mathbf{R}_i) = \mathbf{q}, \mathbf{Z}_i = \mathbf{c}) < 1$ for all $t \in \mathcal{T}$ and $\mathbf{q} \in \mathcal{Q}$, and $\mathbf{z} \in \mathcal{Z}$. In addition, the treatment feature and a deconfounder are separable. By adjusting for such a deconfounder, we can uniquely and nonparametrically identify the marginal distribution of the potential outcome under the treatment condition $T_i = t$ for $t \in \mathcal{T}$ as:

$$\mathbb{P}(Y_i(t, \mathbf{U}_i) = y) = \int_{\mathcal{C}} \int_{\mathcal{R}} \mathbb{P}(Y_i = y \mid T_i = t, \mathbf{f}(\mathbf{R}_i), \mathbf{Z}_i) dF(\mathbf{R}_i) dF(\mathbf{Z}_i)$$

for all $y \in \mathcal{Y}$.

We omit the proof as it is almost identical to the proof of Proposition 1 of Imai and Nakamura (2024).

S2.1.2 Estimation and Inference

Given the identification formula, we next derive the procedure for the estimation and statistical inference. Since our application requires the discrete treatment, we extend the estimation procedure of Imai and Nakamura (2024) to the case of discrete treatment and observed structured confounding variables in this section.

We use the same nuisance functions as in the previous section (i.e., the deconfounder $\mathbf{f}(\mathbf{R}_i)$, the conditional potential outcome $\mu_{T_i}(\mathbf{f}(\mathbf{R}_i), \mathbf{Z}_i)$, and the propensity score $\pi_t(\mathbf{f}(\mathbf{R}_i), \mathbf{Z}_i)$). Our procedure for estimating $\xi(t) = \mathbb{E}[Y_i(t, \mathbf{U}_i)]$ at $T_i = t$ is as follows. Denote the observed data by $\mathcal{D} := \{\mathcal{D}_i\}_{i=1}^N$ where $\mathcal{D}_i := \{Y_i, T_i, \mathbf{R}_i, \mathbf{Z}_i\}$. We use the following K -fold cross-fitting procedure, assuming that N is divisible by K .

1. Randomly partition the data into K folds of equal size where the size of each fold is $n = N/K$. The observation index is denoted by $I(i) \in \{1, \dots, K\}$ where $I(i) = k$ implies that the i th observation belongs to the k th fold.
2. For each fold $k \in \{1, \dots, K\}$, use observations with $I(i) \neq k$ as training data:
 - (a) split the training data into two folds, $I_1^{(-k)}$ and $I_2^{(-k)}$
 - (b) estimate both the deconfounder and the conditional outcome function by solving the optimization problem given in Equation (S2) using the first fold. They are denoted by $\hat{\mathbf{f}}^{(-k)}(\{\mathbf{R}_i, \mathbf{Z}_i\}_{i \in I_1^{(-k)}}) := \mathbf{f}(\{\mathbf{R}_i, \mathbf{Z}_i\}_{i \in I_1^{(-k)}}; \hat{\boldsymbol{\lambda}}^{(-k)})$ and $\hat{\mu}_t^{(-k)}(\{\mathbf{R}_i, \mathbf{Z}_i\}_{i \in I_1^{(-k)}}) := \mu_t(\mathbf{f}(\{\mathbf{R}_i\}_{i \in I_1^{(-k)}}; \hat{\boldsymbol{\lambda}}^{(-k)}), \mathbf{Z}_i; \hat{\boldsymbol{\theta}}^{(-k)})$, respectively, and
 - (c) obtain an estimated propensity score given the estimated deconfounder on the second fold, which is denoted by $\hat{\pi}^{(-k)}(\hat{\mathbf{f}}^{(-k)}(\{\mathbf{R}_i\}_{i \in I_2^{(-k)}}), \mathbf{Z}_i) := \hat{\pi}^{(-k)}(\mathbf{f}(\{\mathbf{R}_i\}_{i \in I_2^{(-k)}}; \hat{\boldsymbol{\lambda}}^{(-k)}), \mathbf{Z}_i)$.
3. For each treatment value $t \in \mathcal{T}$, construct the double debiased ML estimator

$$\hat{\xi}(t) = \frac{1}{nK} \sum_{k=1}^K \sum_{I(i)=k} \left\{ \hat{\mu}_t^{(-k)}(\mathbf{f}(\mathbf{R}_i), \mathbf{Z}_i) + \frac{\mathbb{1}\{T_i = t\}}{\hat{\pi}_t^{(-k)}(\mathbf{f}(\mathbf{R}_i), \mathbf{Z}_i)} \left(Y_i - \hat{\mu}_t^{(-k)}(\mathbf{f}(\mathbf{R}_i), \mathbf{Z}_i) \right) \right\}$$

Under the standard regularity conditions and the Lipschitz continuity of the propensity score function, the procedure above yields the asymptotically normal estimator with the double robustness property.

Model	Facial Traits	Learning Rate	Dropout	Outcome Model	Deconfounder
Stable	Attractiveness	1.081×10^{-7}	0.063	[100, 1]	[512, 256]
Diffusion	Dominance	1.021×10^{-7}	0.270	[200, 1]	[1024, 512]
ver1.5	Trustworthiness	1.166×10^{-7}	0.193	[50, 1]	[512, 256]
Stable	Attractiveness	1.018×10^{-7}	0.083	[100, 1]	[1024, 512]
Diffusion	Dominance	1.019×10^{-7}	0.169	[50, 1]	[512, 256]
ver 2.1	Trustworthiness	1.012×10^{-7}	0.052	[200, 1]	[256, 128]

Table S2: Optimal hyperparameters selected for each independent variable using Optuna for each model. The table lists the learning rate, dropout rate, outcome model architecture, and deconfounder architecture applied to the replication of Lindholm et al. (2024).

S2.2 Implementation Details for the Empirical Application

We reanalyze the dataset originally compiled by Lindholm et al. (2024). In that study, the authors collected facial photographs of Danish political candidates, along with their vote totals and background characteristics — including date of birth, gender, and education — for the 2021 local and 2022 general elections. The initial dataset contained 9,020 candidates. However, the authors excluded individuals whose photos were missing, of low quality, or overlaid with text, as well as those who ran uncontested. This resulted in a final analytic sample of 7,055 candidates. To quantify facial traits, the authors fine-tuned a pre-trained convolutional neural network using the “One Million Impressions” dataset (Peterson et al., 2022), generating estimates for three dimensions of perceived facial characteristics: attractiveness, dominance, and trustworthiness.

We implemented our proposed methodology as follows. First, we padded each image to a square shape with dimensions of 304×304 pixels to ensure uniform input size. We then regenerated the candidate images using Stable Diffusion version 1.5 (Rombach et al., 2022). We extracted the internal representation from the final layer of the diffusion model, prior to the decoder of the variational autoencoder. Consistent with Assumption 3, we made sure that the decoder is a deterministic function of this internal representation.

Unlike in the text-based application, we did not apply a pooling operation to reduce dimensionality. Instead, we flattened the full internal representation (a tensor of shape $16 \times 16 \times 64$) into a single vector of dimension 16,384, which is substantially smaller than the original image size of $304 \times 304 \times 3 = 277,248$.

We estimated both the deconfounder and the outcome model, using this internal representation \mathbf{R} , the treatment feature of interest (one of the three facial traits), the outcome variable (number of votes received), and the structured confounders (age, gender, and education). As some structured confounders were missing, we created the missing indicator variables and interact them with the structured confounders to use the entire data. To evaluate the impact of observed covariates, we fitted the model both with and without these structured confounders.

The neural network architecture used in this application mirrored that of our previous application, and hyperparameter tuning was again performed using Optuna. The tuning procedure followed the same protocol as before, with separate fine-tuning conducted for each of the three facial traits. The selected optimal hyperparameters are reported in Table S2.

To estimate the average potential outcome for each facial trait, we applied the methodology described earlier, using 2-fold cross-fitting in combination with the selected hyperparameters to estimate both the deconfounder and outcome models. All optimization settings — including the choice of optimizer, batch size, number of training epochs, gradient clipping, and early stopping —

were held consistent with the prior application for comparability. We then compared our results to the linear regression results with a discretized treatment and the same covariates, which mirrored the original paper’s analysis in Lindholm et al. (2024).

S3 Structural Model of Texts

In this section, we provide the formal theoretical justification for the methodology introduced in Section 2.3. This application is intended to demonstrate how our GPI framework can be integrated into an existing structural model. Specifically, we tailor the proposed methodology to the experimental setting of Blumenau and Lauderdale (2022), which focuses on estimating the latent persuasiveness of political rhetoric. Unlike the previous two applications, this analysis employs a model-based inferential approach. We begin by outlining the experimental design, then introduce our proposed semiparametric model, and finally detail the implementation of the empirical analysis.

S3.1 Experimental Design

To estimate the latent persuasiveness of political rhetoric, Blumenau and Lauderdale (2022) constructed a set of hypothetical political arguments and randomly assigned pairs of these arguments to survey respondents. The authors designed a total of 336 distinct arguments, which varied systematically across 12 policy issues in contemporary British politics. These arguments served as the treatment conditions in the experiment.

- Building a third runway at Heathrow
- Closing large retail stores on Boxing Day
- Extending the Right to Buy
- Extension of surveillance powers in the UK
- Fracking in the UK
- Nationalization of the railways in the UK
- Quotas for women on corporate boards
- Reducing the legal restrictions on cannabis use
- Reducing university tuition fees
- Renewing Trident
- Spending 0.7% of GDP on overseas aid
- Sugar tax in the UK

and rhetorical elements (14 rhetorical elements):

- Ad hominem
- Appeal to authority
- Appeal to fairness
- Appeal to history
- Appeal to national greatness

<p>Appeal to authority / For</p> <p>The Airports Commission, an independent body established to study the issue, have argued that expanding Heathrow is "the most effective option to address the UK's aviation capacity challenge"</p>
<p>Appeal to history / Against</p> <p>History show us that most large infrastructure projects do not lead to significant economic growth, which suggests that the expansion of Heathrow will fail to pay for itself.</p>

Table S3: Two examples of political rhetorics about the policy issue regarding "Building a third runway at Heathrow."

- Appeal to populism
- Common sense
- Cost and benefit
- Country comparison
- Crisis
- Metaphor
- Morality
- Public opinion
- Side effects of policy

and the side of the argument (2 sides, i.e., for or against).

Once a set of texts were generated, they are randomly assigned to respondents. Specifically, in the experiment, respondents were presented with a pair of randomly selected for and against arguments on the same policy issue, which differ in rhetorical elements. They were then asked to indicate which argument they found more persuasive, or whether they found them equally persuasive. A total of 3,317 respondents participated in the study, and each of them was shown four randomly selected issues, yielding 13,268 observations.

Once the set of arguments was generated, they were randomly assigned to respondents. In the experiment, each respondent was presented with a pair of arguments on the same topic—one in favor and one against a given policy issue—that differed in their rhetorical elements. Respondents were asked to indicate which argument they found more persuasive, or whether they found both equally persuasive. A total of 3,317 respondents participated in the study, each evaluating four randomly selected issue pairs, resulting in 13,268 pairwise observations.

Our goal is to estimate the latent persuasiveness of each rhetorical element. The key methodological challenge is that, although argument pairs are randomly assigned to respondents, the rhetorical elements themselves may still be correlated with other features of the texts. Table S3 provides two example arguments on the same policy issue ("Building a third runway at Heathrow") used in the experiment. While both address the same topic, they differ in multiple dimensions beyond rhetorical style or stance, highlighting the potential for confounding.

To address this issue, Blumenau and Lauderdale (2022) identified seven additional textual features—argument length, readability, positive and negative tone, overall emotional language, fact-based language, and whether the argument was sourced from parliamentary speeches in Hansard

or authored by the researchers—and included them as control variables in their analysis. However, there is no theoretical guarantee that this list fully captures all relevant sources of variation, leaving open the possibility of residual confounding.

S3.2 Model of Latent Persuasiveness

We model the persuasiveness of the political rhetorics in the same way as Blumenau and Lauderdale (2022) but use the internal representation of the deep generative model to adjust for the argument-level confounders. Suppose that we have J arguments indexed by $j = 1, \dots, J$ and N respondents indexed by $i = 1, \dots, N$. Let \mathbf{X}_j denote the text of argument j . We regenerate this text using a deep generative model as defined in Definition 1 and obtain its internal representation \mathbf{R}_j . As before, we assume that the last layer of the deep generative model is a deterministic function of the internal representation \mathbf{R}_j (Assumption 3).

Each argument text \mathbf{X}_j contains three features of interest: a rhetorical element $T_j \in \{1, \dots, 14\}$, a side of the argument $S_j \in \{1, 2\}$ (for or against), and a policy issue $P_j \in \{1, \dots, 12\}$. All features of interest are solely based on the argument text \mathbf{X}_j , and thus can be written as deterministic functions of the internal representation \mathbf{R}_j .

Each respondent i is presented with a pair of arguments $(\mathbf{X}_j, \mathbf{X}_{j'})$ on the same topic $P_j = P_{j'}$ but with the opposite sides $S_j \neq S_{j'}$ and then asked to answer the question about persuasiveness. Let $Y_{jj'(i)}$ denote the outcome variable, representing respondent i 's answer to this question. Then, we can define the outcome as follows:

$$Y_{jj'(i)} = \begin{cases} 0 & \text{if respondent } i \text{ answers that argument } j \text{ is more persuasive} \\ 1 & \text{if respondent } i \text{ answers that both arguments are equally persuasive} \\ 2 & \text{if respondent } i \text{ answers that argument } j' \text{ is more persuasive} \end{cases}$$

We use $\mathcal{J}(i)$ to represent a set of argument pairs assigned to respondent i .

In the original paper, Blumenau and Lauderdale (2022) proposed a model to estimate the latent persuasiveness of the rhetorical elements by adopting the Bradley-Terry model (Bradley and Terry, 1952). The model assumes the following data generating process,

$$\log \left[\frac{\mathbb{P}(Y_{jj'(i)} \leq k)}{\mathbb{P}(Y_{jj'(i)} > k)} \right] = \delta_k + (\alpha_{P_j S_j} + \beta_{T_j} + \gamma_j) - (\alpha_{P_{j'} S_{j'}} + \beta_{T_{j'}} + \gamma_{j'}), \quad (\text{S6})$$

where $\beta_t \sim \mathcal{N}(0, \omega)$ and $\gamma_j \sim \mathcal{N}(0, \sigma_{T_j})$, δ_k is the intercept for response category k , α_{ps} is the fixed effect of the policy issue $P_j = p$ and the side of argument $S_j = s$, β_t is the average effect of the rhetorical element $T_j = t$, and γ_j is the random effect of argument j with variance σ_{T_j} , which varies across rhetorical elements.

While this model has the effect of the policy issue and side of the argument, it does not adjust for the other confounding features of text. The model also assumes that the rhetorical element T_j is linearly separable from policy issues and the side of the argument, and that the prior distributions for β_t and γ_j are independent and normal. Neither assumption is guaranteed by the experimental design. Our goal is to apply GPI and relax these restrictive assumptions.

We estimate the persuasiveness of the rhetorical element T_j in argument j while further adjusting for the confounding features of the text \mathbf{X}_j . As before, let \mathbf{U}_j denote the confounding features of argument j that are not captured by the rhetorical element T_j , policy topic P_j , and side of argument S_j . We assume that these confounding features \mathbf{U}_j are a deterministic function of the argument \mathbf{X}_j , i.e., $\mathbf{U}_j = \mathbf{g}_U(\mathbf{X}_j)$, where \mathbf{g}_U is an unknown vector-valued function (Assumption 8). These confounding features are assumed to be separable from the rhetorical element T_j (Assumption 9).

We model the outcome by relaxing the parameteric assumptions of the original model. Specifically, we assume the following semiparametric structural model:

$$\log \left[\frac{\mathbb{P}(Y_{jj'(i)} \leq y)}{\mathbb{P}(Y_{jj'(i)} > y)} \right] = \delta_y + \mu(T_j, \mathbf{U}_j) - \mu(T_{j'}, \mathbf{U}_{j'}) \quad (\text{S7})$$

where we assume $\sum_{j=1}^J \mu(T_j, \mathbf{U}_j) = 0$ for identification, and $\mu(T_j, \mathbf{U}_j)$ represents the persuasiveness of argument j presented to the respondent i as a function of its rhetorical element T_j and other confounding features \mathbf{U}_j . This model is semiparametric because we do not restrict the functional form of $\mu(T_j, \mathbf{U}_j)$ while assuming that the persuasiveness of argument j does not interact with that of argument j' .

Under this model, we are interested in estimating the persuasiveness of each rhetorical element $T_j = t \in \{1, \dots, 14\}$, which is defined as follows:

$$\beta(t) = \mathbb{E}[\mu(T_j = t, \mathbf{U}_j)]. \quad (\text{S8})$$

Although the confounding features \mathbf{U}_j are unobserved, Proposition 2 shows that we can estimate the quantity of interest by adjusting for the deconfounder $\mathbf{f}(\mathbf{R}_j)$:

$$\beta(t) = \int_{\mathcal{R}} \mu(t, \mathbf{f}(\mathbf{R}_j)) dF(\mathbf{R}_j) \quad (\text{S9})$$

where $\mathbf{f}(\mathbf{R}_j)$ is a function satisfying the conditional independence relation $Y_{jj'(i)} \perp\!\!\!\perp \mathbf{R}_j \mid T_j, \mathbf{f}(\mathbf{R}_j)$. As shown in Proposition 2, the deconfounder function need not be unique.

Based on this identification result, we propose fitting the model with a neural network architecture. Specifically, we use the following semiparametric structural model for estimation:

$$\log \left[\frac{\mathbb{P}(Y_{jj'(i)} \leq k)}{\mathbb{P}(Y_{jj'(i)} > k)} \right] = \delta_k + \mu(T_j, \mathbf{f}(\mathbf{R}_j; \boldsymbol{\lambda}); \boldsymbol{\theta}) - \mu(T_{j'}, \mathbf{f}(\mathbf{R}_{j'}; \boldsymbol{\lambda}); \boldsymbol{\theta}). \quad (\text{S10})$$

where $\boldsymbol{\lambda}$ and $\boldsymbol{\theta}$ are the parameters of the deconfounder function $\mathbf{f}(\mathbf{R}_j; \boldsymbol{\lambda})$ and the argument persuasiveness function $\mu(T_j, \mathbf{f}(\mathbf{R}_j; \boldsymbol{\lambda}); \boldsymbol{\theta})$, respectively, and $\sum_{j=1}^J \mu(T_j, \mathbf{f}(\mathbf{R}_j; \boldsymbol{\lambda}); \boldsymbol{\theta}) = 0$. This structural model is feasible because we observe the internal representation \mathbf{R}_j , which enables us to estimate both the deconfounder $\mathbf{f}(\mathbf{R}_j)$ and the function $\mu(T_j, \mathbf{f}(\mathbf{R}_j))$.

We model $\mu(T_j, \mathbf{f}(\mathbf{R}_j; \boldsymbol{\lambda}); \boldsymbol{\theta})$ as a neural network function of the deconfounder $\mathbf{f}(\mathbf{R}_j)$ and the treatment feature T_j , using the architecture introduced in the previous section (Figure S2). This neural network architecture encodes the conditional independence relationship $Y_{jj'(i)} \perp\!\!\!\perp \mathbf{R}_j \mid T_j, \mathbf{f}(\mathbf{R}_j)$. We minimize the following loss function to estimate the parameters:

$$\begin{aligned} \{\hat{\boldsymbol{\lambda}}, \hat{\boldsymbol{\theta}}, \hat{\boldsymbol{\delta}}\} = \underset{\boldsymbol{\lambda}, \boldsymbol{\theta}, \boldsymbol{\delta}}{\operatorname{argmin}} & - \sum_{i=1}^N \sum_{(j, j') \in \mathcal{J}(i)} \sum_{k=0}^1 [\mathbb{1}\{Y_{jj'(i)} \leq k\} \log \sigma(\delta_k + \mu_{jj'}) + \mathbb{1}\{Y_{jj'(i)} > k\} \log \{1 - \sigma(\delta_k + \mu_{jj'})\}] \\ \text{s.t.} & \sum_{j=1}^J \mu(T_j, \mathbf{f}(\mathbf{R}_j; \boldsymbol{\lambda}); \boldsymbol{\theta}) = 0, \end{aligned} \quad (\text{S11})$$

where $\mu_{jj'} = \mu(T_j, \mathbf{f}(\mathbf{R}_j; \boldsymbol{\lambda}); \boldsymbol{\theta}) - \mu(T_{j'}, \mathbf{f}(\mathbf{R}_{j'}; \boldsymbol{\lambda}); \boldsymbol{\theta})$ and $\sigma(x) = 1/(1 + \exp(-x))$ is the logistic function. Once we estimate the parameters $\boldsymbol{\lambda}$ and $\boldsymbol{\theta}$, we can compute the estimated persuasiveness of each rhetorical element $T_j = t \in \{1, \dots, 14\}$ using Equation (S9). We quantify the uncertainty of the estimated persuasiveness using the Monte Carlo dropout method (Gal and Ghahramani, 2016).

The entire estimation procedure can be summarized as follows.

Model	dim(\mathbf{R})	Learning Rate	Dropout	Outcome Model	Deconfounder
LLaMA3 (8B)	4096	9.626×10^{-5}	0.294	[50, 1]	[256, 128]
LLaMA3.3 (70B)	8192	9.967×10^{-5}	0.152	[50, 1]	[512, 256]
Gemma3 (1B)	1152	9.916×10^{-5}	0.280	[50, 1]	[1024, 512]

Table S4: Optimal hyperparameters selected for the outcome model and deconfounder in the replication of Blumenau and Lauderdale (2022). The table lists the learning rate, dropout rate, outcome model architecture, and deconfounder architecture.

1. Use the entire data to solve the optimization problem given in Equation (S11) and simultaneously obtain $\hat{\mathbf{f}}(\mathbf{R}_j) := \mathbf{f}(\mathbf{R}_j; \hat{\boldsymbol{\lambda}})$ and $\hat{\mu}(T_j, \mathbf{R}_j) := \mu(T_j, \mathbf{f}(\mathbf{R}_j; \hat{\boldsymbol{\lambda}}); \hat{\boldsymbol{\theta}})$
2. Obtain the estimated latent persuasiveness of each rhetorical element $t \in \{1, \dots, 14\}$ by

$$\hat{\beta}(t) = \frac{1}{J} \sum_{j=1}^J \hat{\mu}(t, \hat{\mathbf{f}}(\mathbf{R}_j)), \quad (\text{S12})$$

and the uncertainty quantification with Monte Carlo dropout.

S3.3 Implementation Details of the Empirical Application

To implement our proposed methodology, we first regenerated all 336 arguments used in the experiment of Blumenau and Lauderdale (2022) using the three different LLMs: (1) LLaMA3 with 8 billion parameters, (2) LLaMA3.3 with 8 billion parameters, and (3) Gemma 3 with 1 billion parameters. Similar to the first application, we extracted the internal representation of each argument. The dimensions of internal representation \mathbf{R}_i are different across models: 4096 for LLaMA3 with 8 billion parameters, 8192 for LLaMA3.3 with 70 billion parameters, and 1152 for Gemma 3 with 1 billion parameters. Even though the dimensions are different, since all internal representations deterministically regenerate each arguments, they should contain all the information contained in the texts and should yield the similar estimates. Using the same neural network architecture as in the previous two applications, we fine-tuned both the outcome model and the deconfounder within the semiparametric structural model (see Equation (S10)). We implemented the constraint in the optimization problem (Equation (S11)) by demeaning the estimated outcome model, ensuring its average is zero.

For fine-tuning, we employed the same hyperparameter search space and procedure as in the previous two applications, optimizing the hyperparameters using Optuna. For both fine-tuning and the entire structural model fitting, we used the Adam optimizer with batch size of 256 and weight decay of 10^{-8} , and we applied gradient clipping with a maximum norm of 1.0. The optimal hyperparameters selected by Optuna are shown in Table S4. We then fitted the entire structural model using the selected hyperparameters and a 2-fold cross-fitting procedure, as described above. Once we had fitted the outcome model, we estimated the latent persuasiveness based on Equation (S12) and its uncertainty using Monte Carlo dropout with 3000 samples.

We find that the estimated latent persuasiveness of rhetorical elements is consistent across the three LLMs, as shown in Figure S4. The Pearson’s correlation for the estimated latent persuasiveness of rhetorical elements across models are 0.89 for LLaMA 3 (8B) and LLaMA 3.3 (70B), 0.97 for LLaMA 3 (8B) and Gemma 3 (1B), and 0.86 for LLaMA 3.3 (70B) and Gemma 3 (1B). These results suggest that even though the internal representations are different, the three LLMs yield similar estimates under the deterministic decoding assumption (Assumption 3).

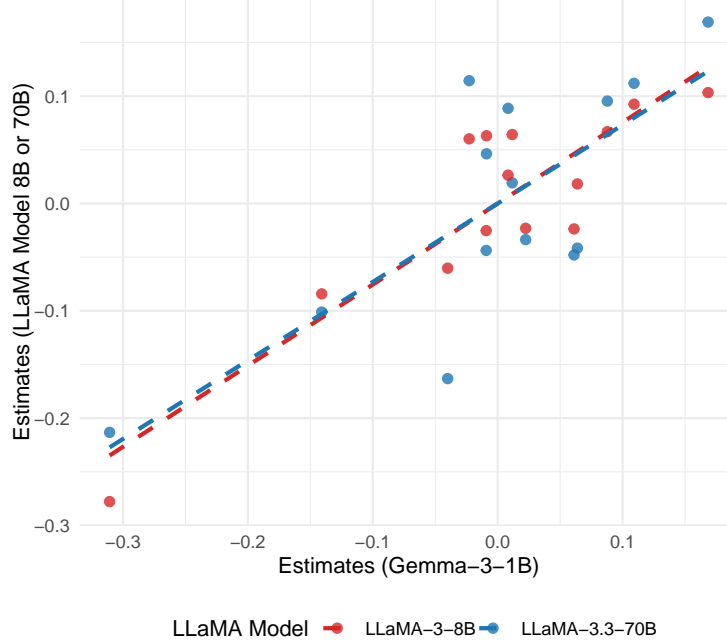


Figure S4: The estimated latent persuasiveness of rhetorical elements across three LLMs (LLaMA3 with 8 billion parameters, LLaMA 3.3 with 70 billion parameters, and Gemma 3 with 1 billion parameters). The dashed lines represent the fitted regression lines.

S4 Proof of Proposition 1

Proof Under the definition of the deep generative model (see Definition 1) and Assumption 3, we can write $\mathbf{U}_i = \mathbf{f}^*(\mathbf{R}_i)$ with some deterministic function \mathbf{f}^* . Then,

$$\begin{aligned}
\mathbb{P}(Y_i(t) = y) &= \int_{\mathcal{Z}} \int_{\mathcal{U}} \mathbb{P}(Y_i(t) = y \mid \mathbf{Z}_i, \mathbf{U}_i) dF(\mathbf{U}_i) dF(\mathbf{Z}_i) \\
&= \int_{\mathcal{Z}} \int_{\mathcal{U}} \mathbb{P}(Y_i(t) = y \mid T_i = t, \mathbf{Z}_i, \mathbf{U}_i) dF(\mathbf{U}_i) dF(\mathbf{Z}_i) \\
&= \int_{\mathcal{Z}} \int_{\mathcal{U}} \mathbb{P}(Y_i = y \mid T_i = t, \mathbf{Z}_i, \mathbf{U}_i) dF(\mathbf{U}_i) dF(\mathbf{Z}_i) \\
&= \int_{\mathcal{Z}} \int_{\mathcal{U}} \mathbb{P}(Y_i = y \mid T_i = t, \mathbf{Z}_i, \mathbf{f}^*(\mathbf{R}_i)) dF(\mathbf{f}^*(\mathbf{R}_i)) dF(\mathbf{Z}_i) \\
&= \int_{\mathcal{Z}} \int_{\mathbb{R}^q} \mathbb{P}(Y_i = y \mid T_i = t, \mathbf{Z}_i, \mathbf{f}^*(\mathbf{R}_i)) dF(\mathbf{R}_i) dF(\mathbf{Z}_i)
\end{aligned}$$

where the second equality follows from Assumption 2, the third equality follows from Assumption 1. Finally, suppose that there exists another function $\mathbf{f}(\mathbf{R}_i)$ that satisfies the conditional independence relation $Y_i \perp\!\!\!\perp \mathbf{R}_i \mid T_i, \mathbf{Z}_i, \mathbf{f}(\mathbf{R}_i)$. Then,

$$\begin{aligned}
&\int_{\mathcal{Z}} \int_{\mathbb{R}^q} \mathbb{P}(Y_i = y \mid T_i = t, \mathbf{Z}_i, \mathbf{f}(\mathbf{R}_i)) dF(\mathbf{R}_i) dF(\mathbf{Z}_i) \\
&= \int_{\mathcal{Z}} \int_{\mathbb{R}^q} \mathbb{P}(Y_i = y \mid T_i = t, \mathbf{Z}_i, \mathbf{f}(\mathbf{R}_i), \mathbf{R}_i) dF(\mathbf{R}_i) dF(\mathbf{Z}_i)
\end{aligned}$$

$$\begin{aligned}
&= \int_{\mathcal{Z}} \int_{\mathbb{R}^q} \mathbb{P}(Y_i = y \mid T_i = t, \mathbf{Z}_i, \mathbf{f}^*(\mathbf{R}_i), \mathbf{R}_i) dF(\mathbf{R}_i) dF(\mathbf{Z}_i) \\
&= \int_{\mathcal{Z}} \int_{\mathbb{R}^q} \mathbb{P}(Y_i = y \mid T_i = t, \mathbf{Z}_i, \mathbf{f}^*(\mathbf{R}_i)) dF(\mathbf{R}_i) dF(\mathbf{Z}_i)
\end{aligned}$$

Thus, any function of \mathbf{R}_i that satisfies the conditional independence relation $Y_i \perp\!\!\!\perp \mathbf{R}_i \mid T_i, \mathbf{Z}_i, \mathbf{f}(\mathbf{R}_i)$ leads to the same identification formula. \square